machines

MDPI

Article

Prescribed-Time Formation Tracking Control of Fixed-Wing UAVs with Disturbance and Failures

Gongxian Lou and Maolong Lv *

School of Air Traffic Control and Navigation, Air Force Engineering University, Xi'an 710051, China; 18829501370@163.com

* Correspondence: maolonglv@163.com

Abstract

This paper proposes a novel prescribed-time formation tracking control farmework of multi-fixed-wing UAVs under external disturbance and actuator failures. As the complexity of aerial missions intensifies, achieving precise position and attitude tracking within a user-defined upper bound of settling time becomes a paramount challenge for intelligent swarm systems. Unlike traditional finite or fixed-time methods, where convergence depends on initial states or suffers from conservative estimation, the proposed approach ensures stability within a prescribed time independent of initial conditions. A key innovation is the introduction of a piecewise reference convergence differential function. This mechanism eliminates the need for state transitions, thereby reducing computational complexity while ensuring smooth tracking without control surface chattering across the entire mission. Additionally, a prescribed-time sliding mode disturbance observer is developed to provide precise and timely compensation for external disturbances and actuator faults. Rigorous Lyapunov analysis proves that all closed-loop signals are bounded and the tracking errors converge to a small neighborhood of zero within the predefined time. Numerical simulations demonstrate that, under time-varying disturbances and actuator faults, the disturbance estimation errors converge within 4 s, while both attitude and velocity tracking errors converge within 6 s, achieving fast transient response and high tracking accuracy. The UAV swarm successfully maintains the desired formation during aggressive maneuvers, including speed variations, climbing, and diving. These results verify that the proposed method provides a computationally efficient, robust, and high-precision solution for time-critical formation control of fixed-wing UAV swarms under complex uncertainties.

Keywords: prescribed-time stability; tracking control; sliding mode control; fixed-wing UAV swarm; non-vanishing uncertainties

Check for updates

Academic Editor: Tao Li

Received: 20 April 2026
Revised: 7 May 2026
Accepted: 11 May 2026
Published: 12 May 2026

Copyright: © 2026 by the authors. Licensee MDPI, Basel, Switzerland. This article is an open access article distributed under the terms and conditions of the Creative Commons Attribution (CC BY) license.

1. Introduction

As the exploration of aerial domains intensifies, the flight control technology for fixed-wing unmanned aerial vehicle (UAV) swarms has seen rapid development and become a focal point in both military and civil applications [1]. Compared with single aircraft or rotorcraft [2], fixed-wing UAV swarms offer distinct advantages such as high cruise speeds, extended endurance, and the ability to cover vast geographical areas, making them indispensable for large-scale tasks such as persistent wide-area surveillance [3], long-range collaborative strikes [4], and atmospheric research [5]. In a swarm configuration, the necessity to maintain strict formation geometry while adapting to high-speed maneuvers requires each agent to achieve simultaneous and precise position and attitude tracking

control [6,7]. Meanwhile, in complex mission, fixed-wing UAV swarms need to face not only external disturbances but also the stringent requirements of time-critical coordination [8,9]. Thus, against unknown disturbances and model uncertainties, how to achieve precise position and attitude tracking within an accurate, user-defined UST becomes a paramount challenge for the next generation of intelligent swarm systems.

In swarm missions, position tracking ensures the spatial coordination and collision avoidance, while attitude tracking is the prerequisite for generating the necessary aerodynamic lift and maintaining flight stability [10]. Currently, various control methods have been designed from aspects such as trajectory tracking accuracy and the upper bound of settling time (UST), including PID control [9,11,12], neural network control [13–16], and sliding mode control (SMC) [17], achieving fruitful research outcomes. Among these methods, SMC has garnered widespread attention due to its strong robustness against uncertainties and disturbances. It is worth noting that traditional sliding mode control can only guarantee asymptotic stability and cannot provide an accurate upper bound of settling time [18–20]. In practical control engineering for UAV swarms, there are special tasks that need to be completed within a specified time, such as rapid formation assembly and emergency obstacle avoidance. Failure to meet the above requirements can result in significant losses or collisions between aircraft. To address this issue, finite-time terminal sliding mode control methods have been applied to various aerial vehicles, achieving good control effects [21,22]. However, the convergence time of finite-time stability is usually related to the system's initial state, which may be difficult to obtain or even impossible to measure in a dynamic swarm environment. To solve this problem, fixed-time control (FxTC) was investigated to make the convergence time independent of the initial state. Compared with finite-time control, FxTC has faster transient response and convergence speed [23,24]. By combining SMC with FxTC, fixed-time sliding mode control (FxTSMC) has been verified on many experimental platforms. However, when the system state is in the singular region, most current research solves the singularity problem by switching the controller into other function forms. Thus, considering a more direct way to solve the singularity problem is urgent. Meanwhile, although FxTC offers advantages, the UST obtained through it is still conservative and has a complex relationship with controller parameters. Considering the rigorous application requirements of fixed-wing swarms, prescribed-time stability (PTS) has been introduced, allowing users to pre-set the UST [25,26]. However, many existing methods only guarantee prescribed-time stability in the reaching phase without considering the sliding phase, or vice-versa [27,28]. In addition, the lemmas for prescribed stability in the literature are often relatively strict, making it difficult to combine with other algorithms to solve practical position–attitude coordination problems [29,30]. Therefore, an SMC scheme with prescribed-time convergence in both the sliding and reaching phases is an interesting approach to achieve tracking control.

Furthermore, previous prescribed-time controls (PTC) usually adopt state transitions with time-scaling functions, inevitably causing tedious calculations that are unfavorable for the onboard processors of fixed-wing UAVs. To overcome this defect, control strategies using reference convergence differential functions (RCDFs) have been explored [31]. However, existing PTC schemes without state transitions are merely proposed for specific nonlinear systems, and their scope of application is limited. Establishing a PTC without state transition for the position and attitude of fixed-wing UAV swarms to reduce calculation is worthy of study. It is crucial to recognize that most current PTC methods primarily address regulation within a specified time and do not extend beyond it. Although some approaches are applicable over the entire time interval, they involve switching mechanisms that can lead to non-smooth behavior and chattering in the UAV's control surfaces. Consequently, it is important to explore a new approach that avoids transition mechanisms and enables

the system to maintain effective tracking control throughout the entire time interval. For clarity of presentation, existing studies are systematically summarized in Table 1.

Table 1. Summary of existing control approaches and problem definition.

Approach	Key Findings	Advantages	Disadvantages
Traditional Sliding Mode Control (SMC) [17–20]	Utilizes a sliding manifold to drive system states to equilibrium.	Shows strong robustness against uncertainties and disturbances.	Can only guarantee asymptotic stability and cannot provide an accurate upper bound of settling time (UST).
Finite-time terminal SMC [21,22]	Introduces finite-time stability into traditional SMC.	Meets requirements for tasks needing completion within a specified time.	The convergence time is related to the system's initial state, which may be difficult or impossible to measure in dynamic swarm environments.
Fixed-time control (FxTC) [23,24] & FxTSMC	Investigated to make the convergence time independent of the initial state.	Has faster transient response and convergence speed compared with finite-time control.	The obtained UST is still conservative and has a complex relationship with controller parameters.
Traditional Prescribed-time control (PTC) [25–28]	Investigated to make the convergence time strictly depend on a user-defined threshold.	Allows users to accurately pre-set the Upper bound of Settling Time (UST).	Usually adopts state transitions causing tedious calculations, non-smooth behavior, and control surface chattering.

On the other hand, due to the disturbance of complex and unpredictable aerial environments, such as stochastic wind gusts, atmospheric turbulence, and varying air densities, and the inherent model uncertainties like aerodynamic coefficient disturbance, the issue of how to make fixed-wing UAV swarms move along the desired trajectories has been extensively studied [32,33]. To solve this, sliding-mode disturbance observers (SMDOs) are favored for their ability to estimate and compensate for dynamic disturbances. However, existing finite-time and fixed-time SMDOs provide a rough estimation time; this time is still affected by the initial values and observer parameters [34,35]. In the observer-based prescribed-time control framework, the coordination between the controller and the observer is a key factor. Thus, it is also indispensable to design a prescribed-time sliding mode disturbance observer (PTSMDO).

- Unlike existing finite-time or fixed-time control methods [18–24], which are often limited by dependence on initial states or conservative estimation and fail to ensure prescribed-time convergence in both the reaching and sliding phases, a prescribed-time sliding mode control architecture for fixed-wing UAVs is proposed based on the prescribed-time stability mechanism. This architecture achieves prescribed-time tracking throughout the entire process of both phases, resulting in high-precision control where the convergence time is completely decoupled from initial conditions and can be accurately pre-defined by the user.
- Compared with existing prescribed-time controls [25–30] that rely on complex time-scaling functions for segmented switching, a novel continuous and smooth piecewise reference convergence differential function is introduced to provide a more versatile approach. By employing this PRCDF, the system achieves a flexible convergence rate for tracking errors while avoiding state transitions in the controller design. This

mechanism seamlessly maintains tracking effectiveness over the entire time interval, which substantially lowers computational complexity.

- In contrast to existing sliding mode observers [32–35], where estimation time is highly sensitive to environmental disturbances and initial conditions cannot be determined a priori, a prescribed-time sliding mode disturbance observer is proposed. This observer is designed by integrating an integral sliding mode with a prescribed-time convergence operator. Rapid and accurate online estimation of unknown complex aerodynamic disturbances and actuator faults is achieved. Furthermore, full disturbance compensation is completed before the convergence of the controller states, leading to a significant improvement in system tracking accuracy under strong interference environments.

The rest of this article unfolds as follows. The problem formulation and preliminaries are introduced in Section 2. In Section 3, the prescribed-time formation tracking control strategy integrated with a sliding mode disturbance observer is synthesized. The numerical simulations and hardware-in-the-loop experiments are presented in Section 4 to verify the theoretical findings. Conclusion and discussion are summarized in Section 5.

2. Problem Formulation and Preliminaries

2.1. Fixed-Wing UAV Modeling

Let us start by considering a formation of fixed-wing UAVs, which includes one leader and a group of N followers. As per the architectural descriptions in [1], the six-degree-of-freedom (6-DOF) dynamics for any i-th UAV (indexed as $i \in \{0, 1, \ldots, N\}$) is visualized in Figure 1 and can be formulated as follows:

$$\begin{cases} \dot{\boldsymbol{p}}_i = \boldsymbol{R}_1(\boldsymbol{\varphi}_i)\boldsymbol{v}_i, \\ \dot{\boldsymbol{v}}_i = -\boldsymbol{S}(\boldsymbol{\omega}_i)\boldsymbol{v}_i + \frac{\boldsymbol{F}_{Ti}}{m_i} + \boldsymbol{R}_1^{\mathrm{T}}(\boldsymbol{\varphi}_i)\boldsymbol{g} + \frac{\boldsymbol{F}_{ai}}{m_i} + \boldsymbol{d}_{vi}, \\ \dot{\boldsymbol{\varphi}}_i = \boldsymbol{R}_2^{-1}(\boldsymbol{\varphi}_i)\boldsymbol{\omega}_i, \\ \boldsymbol{J}_i\dot{\boldsymbol{\omega}}_i = -\boldsymbol{\omega}_i \times \boldsymbol{J}_i\boldsymbol{\omega}_i + \boldsymbol{F}_{bi} + \boldsymbol{C}_i\boldsymbol{\delta}_i + \boldsymbol{J}_i\boldsymbol{d}_{wi}, \end{cases} \tag{1}$$

where $\boldsymbol{\varphi}_i = [\phi_i, \theta_i, \psi_i]^{\mathrm{T}}$ denotes the attitude vector (roll, pitch, and yaw), while $\boldsymbol{v}_i = [u_i, v_i, V_i]^{\mathrm{T}}$ and $\boldsymbol{p}_i = [x_i, y_i, z_i]^{\mathrm{T}}$ signify the body-frame linear velocity and the inertial-frame position, respectively. The control inputs for the system consist of $\boldsymbol{\delta}_i = [\delta_{xi}, \delta_{yi}, \delta_{zi}]^{\mathrm{T}}$ and the thrust vector $\boldsymbol{F}_{Ti} = [F_{Txi}, 0, 0]^{\mathrm{T}}$. Furthermore, let m_i be the UAV's mass and $\boldsymbol{g} = [0, 0, g]^{\mathrm{T}}$ represent the gravitational acceleration. The matrices $\boldsymbol{R}_2(\cdot)$ and $\boldsymbol{R}_1(\cdot)$ are defined as the mapping from Euler rate to angular velocity and the transformation from body to inertial coordinates, respectively. Define $\boldsymbol{J}_i$ as the inertia tensor matrix, assuming symmetry across the $x-z$ plane. These matrices are explicitly structured as:

$$\begin{aligned} \boldsymbol{R}_1 &= \begin{bmatrix} cos_{\psi i}c_{\theta i} & -s_{\psi i}s_{\phi i} + c_{\psi i}s_{\theta i}s_{\phi i} & s_{\psi i}s_{\phi i} + c_{\psi i}s_{\theta i}c_{\phi i} \\ s_{\psi i}c_{\theta i} & c_{\psi i}c_{\phi i} + s_{\psi i}s_{\theta i}s_{\phi i} & -c_{\psi i}s_{\phi i} + s_{\psi i}s_{\theta i}c_{\phi i} \\ -s_{\theta i} & c_{\theta i}s_{\phi i} & c_{\theta i}c_{\phi i} \end{bmatrix}, \\ \boldsymbol{R}_2 &= \begin{bmatrix} 1 & 0 & -s_{\psi i} \\ 0 & c_{\psi i} & s_{\psi i}c_{\theta i} \\ 0 & -s_{\theta i} & c_{\psi i}c_{\theta i} \end{bmatrix}, \quad \boldsymbol{J}_i = \begin{bmatrix} J_{xxi} & 0 & -J_{xzi} \\ 0 & J_{yyi} & 0 \\ -J_{zxi} & 0 & J_{zzi} \end{bmatrix}, \end{aligned} \tag{2}$$

where the trigonometric terms $\cos(\cdot)$ and $\sin(\cdot)$ are abbreviated as c. and s., respectively. Regarding the aerodynamic effects, $\boldsymbol{F}_{bi}$ and $\boldsymbol{F}_{ai}$ refer to the moments and forces, expressed as $F_{ai} = \bar{q}_i S_i R_3(\alpha_i, \beta_i)^{-1}[-C_{D_i}, C_{Y_i}, -C_{L_i}]^{\mathrm{T}}$, $F_{bi} = \bar{q}_i S_i [bC_{l_i}, \hat{c}C_{m_i}, bC_{n_i}]^{\mathrm{T}}$, where the geometric parameters $S_i, \hat{c}_i, b_i$ denote the wing area, mean aerodynamic chord, and wingspan. The dynamic pressure is defined as $\bar{q}_i = \frac{1}{2}\bar{\kappa}V_i^2$, in which $\bar{\kappa}$ is the density of air and $V_i = \|v_i\|$ is the magnitude of the total velocity. Reference [36] provides the dimensionless coefficients

C_{k_i} for $k \in \{l, m, n, D, Y, L\}$. The transformation matrix $\boldsymbol{R}_3(\cdot)$, which relates the body frame to the virtual wind frame based on relative motion, is given by:

$$\boldsymbol{R}_3 = \begin{bmatrix} c_{\alpha i}c_{\beta i} & s_{\beta i} & s_{\alpha i}c_{\beta i} \\ -c_{\alpha i}s_{\beta i} & c_{\beta i} & -s_{\alpha i}s_{\beta i} \\ -s_{\alpha i} & 0 & c_{\alpha i} \end{bmatrix}, \tag{3}$$

where the sideslip angle $\beta_i = \arcsin(v_i/V_i)$ and the angle of attack $\alpha_i = \arctan(V_{\varphi i}/u_i)$ are defined. The control effectiveness is determined by the gain matrix $\boldsymbol{C}_i$:

$$\boldsymbol{C}_i = \bar{q}_i S_i \begin{bmatrix} b_i C_{l\delta ai} & 0 & b_i C_{l\delta ri} \\ 0 & \bar{c}_i C_{m\delta ei} & 0 \\ b_i C_{n\delta ai} & 0 & b_i C_{n\delta ri} \end{bmatrix}. \tag{4}$$

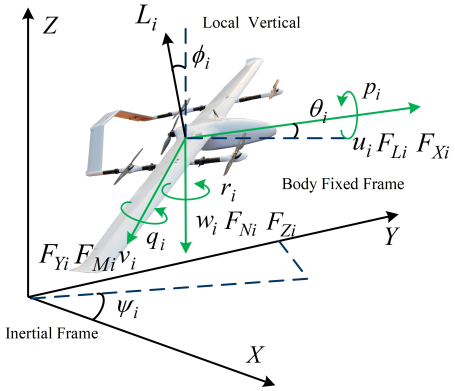


Figure 1. 6-DoF fixed-wing UAV model.

The operator $\boldsymbol{S}(\omega_i)$ denotes the skew-symmetric cross-product matrix. For the follower set $i \in \{1, \ldots, N\}$, external disturbances affecting the rotational and translational subsystems are represented by $\boldsymbol{d}_{V_{\varphi i}}$ and $\boldsymbol{d}_{v_i}$, respectively, which are assumed to be bounded but unknown. Regarding the leader (UAV 0), we assume the disturbances $\boldsymbol{d}_{w0}$ and $\boldsymbol{d}_{v0}$ are zero, while $\boldsymbol{F}_{b0}$ and $\boldsymbol{F}_{a0}$ are treated as known parameters.

2.2. Modeling of Disturbance and Actuator Failures

(1) Translational kinematics: Differentiating the relation $\boldsymbol{\omega}_i = \boldsymbol{R}_2(\boldsymbol{\varphi}_i)\dot{\boldsymbol{\varphi}}_i$ leads to the expression $\dot{\omega}_i = \dot{R}_2(\varphi_i)\dot{\varphi}_i + R_2(\varphi_i)\ddot{\varphi}_i$. By substituting this into (8), the second-order derivative of the Euler angles is obtained as:

$$\ddot{\boldsymbol{\varphi}}_i = (\boldsymbol{J}_i\boldsymbol{R}_2)^{-1}\boldsymbol{C}_i\boldsymbol{\delta}_i + (\boldsymbol{J}_i\boldsymbol{R}_2)^{-1}\left(-\boldsymbol{J}_i\dot{\boldsymbol{R}}_2\dot{\boldsymbol{\varphi}}_i + \boldsymbol{S}(\boldsymbol{J}_i\boldsymbol{R}_2\dot{\boldsymbol{\varphi}}_i)\boldsymbol{R}_2\dot{\boldsymbol{\varphi}}_i + \boldsymbol{F}_{b_i} + \boldsymbol{J}_i\boldsymbol{d}_{\varphi_i}\right). \tag{5}$$

Considering the intricacies of flight environments, parameters such as aerodynamic coefficients and rotational inertia inevitably exhibit uncertainties. Consequently, we decompose terms like $(\boldsymbol{J}_i\boldsymbol{R}_2)^{-1}\boldsymbol{F}_{b_i}$, $(\boldsymbol{J}_i\boldsymbol{R}_2)^{-1}\boldsymbol{S}(\boldsymbol{J}_i\boldsymbol{R}_2\dot{\boldsymbol{\varphi}}_i)\boldsymbol{R}_2\dot{\boldsymbol{\varphi}}_i$, and $(\boldsymbol{J}_i\boldsymbol{R}_2)^{-1}\boldsymbol{C}_i\boldsymbol{\delta}_i$ into their nominal components: $(\boldsymbol{J}_{0i}\boldsymbol{R}_2)^{-1}\boldsymbol{F}_{b_i}$, $(\boldsymbol{J}_{0i}\boldsymbol{R}_2)^{-1}\boldsymbol{S}(\boldsymbol{J}_{0i}\boldsymbol{R}_2\dot{\boldsymbol{\varphi}}_i)\boldsymbol{R}_2\dot{\boldsymbol{\varphi}}_i$, $(\boldsymbol{J}_{0i}\boldsymbol{R}_2)^{-1}\boldsymbol{C}_{0i}\boldsymbol{\delta}_i$, and the corresponding perturbed terms: $\Delta\big((\boldsymbol{J}_i\boldsymbol{R}_2)^{-1}\boldsymbol{F}_{b_i}\big)$, $\Delta\big((\boldsymbol{J}_i\boldsymbol{R}_2)^{-1}\boldsymbol{S}(\boldsymbol{J}_i\boldsymbol{R}_2\dot{\boldsymbol{\varphi}}_i)\boldsymbol{R}_2\dot{\boldsymbol{\varphi}}_i\big)$, and $\Delta\big((\boldsymbol{J}_i\boldsymbol{R}_2)^{-1}\boldsymbol{C}_i\big)\boldsymbol{\delta}_i$.

Furthermore, we account for potential rudder anomalies during actual operation. Individual failure models are formulated for the elevator, ailerons, and rudder:

$$\boldsymbol{\delta}_i = \boldsymbol{\varrho}_{\delta_i}\boldsymbol{\delta}_{i0} + \boldsymbol{\delta}_{if}, \tag{6}$$

where the nominal control command is $\boldsymbol{\delta}_{i0} = [\delta_{xi0}, \delta_{yi0}, \delta_{zi0}]^{\mathrm{T}}$, and the unknown bias fault is $\boldsymbol{\delta}_{if} = [\delta_{xif}, \delta_{yif}, \delta_{zif}]^{\mathrm{T}}$. The term $\boldsymbol{\varrho}_{\delta_i} = \mathrm{diag}\{\varrho_{\delta xi}, \varrho_{\delta yi}, \varrho_{\delta zi}\}$ represents the efficiency factor of

the actuators with three cases: (i) fault-free: $\varrho_{\delta ji} = 1, \delta_{jif} = 0$; (ii) partial loss of effectiveness: $\varrho_{\delta ji} \in (0,1), \delta_{jif} = 0$; (iii) bias fault: $\varrho_{\delta ji} = 1, \delta_{jif} \neq 0$.

Based on parameter uncertainties and rudder failures, the whole rotational dynamics (1) can be rewritten as:

$$\begin{bmatrix} \dot{\boldsymbol{\varphi}}_i \\ \ddot{\boldsymbol{\varphi}}_i \end{bmatrix} = \begin{bmatrix} \mathbf{0}_{3\times3} & \boldsymbol{I}_3 \\ \mathbf{0}_{3\times3} & \mathbf{0}_{3\times3} \end{bmatrix} \begin{bmatrix} \boldsymbol{\varphi}_i \\ \dot{\boldsymbol{\varphi}}_i \end{bmatrix} + \begin{bmatrix} \mathbf{0}_{3\times3} \\ B_{i1}\boldsymbol{\varrho}_{\delta_i} \end{bmatrix} \boldsymbol{\delta}_{i0} + \begin{bmatrix} \mathbf{0}_{3\times3} \\ B_{i2} + B_{i3} \end{bmatrix}, \tag{7}$$

where $B_{i1} = (J_{i0}R_2)^{-1}C_{i0}$ and $B_{i2} = (J_{i0}R_2)^{-1}F_{b_i} - R_2^{-1}\dot{R}_2\dot{\boldsymbol{\varphi}}_i + (J_{i0}R_2)^{-1}S(J_{i0}R_2\dot{\boldsymbol{\varphi}}_i)R_2\dot{\boldsymbol{\varphi}}_i$ are known function terms, $B_{i3} = \Delta\big((J_iR_2)^{-1}S(J_iR_2\dot{\boldsymbol{\varphi}}_i)R_2\dot{\boldsymbol{\varphi}}_i\big) + \Delta\big((J_iR_2)^{-1}F_{b_i}\big) + \Delta\big((J_iR_2)^{-1}C_i\big)\boldsymbol{\delta}_i + R_2^{-1}\boldsymbol{d}_{\omega_i} + (J_{i0}R_2)^{-1}C_{i0}\boldsymbol{\delta}_{if}$ is an uncertain function term.

With $\dot{\varphi}_i = \boldsymbol{M}_i$, we have:

$$\begin{cases} \dot{\boldsymbol{\varphi}}_i = \boldsymbol{M}_i \\ \ddot{\boldsymbol{\varphi}}_i = \boldsymbol{B}_{i1}\delta_{i0} + \boldsymbol{D}_{\varphi i} \end{cases} \tag{8}$$

where $\boldsymbol{D}_{\varphi i} = \boldsymbol{B}_{i2} + \boldsymbol{B}_{i3} + \boldsymbol{B}_{i1}(\boldsymbol{\rho}_{\delta i} - \boldsymbol{I}_3)\delta_{i0}$.

(2) Translational kinematics: According to dynamic (1) and the definition of V_i, the derivative of scalar speed is obtained that:

$$\dot{V}_i = \frac{\boldsymbol{v}_i^{\mathrm{T}}\dot{\boldsymbol{v}}_i}{V_i} = \frac{\boldsymbol{v}_i^{\mathrm{T}}}{V_i}\left(-\boldsymbol{S}(\boldsymbol{w}_i)\boldsymbol{v}_i + \frac{F_{T_i}}{m_i} + R_1^{\mathrm{T}}(\boldsymbol{\varphi}_i)\boldsymbol{g} + \frac{F_{a_i}}{m_i} + \boldsymbol{d}_{v_i}\right). \tag{9}$$

In order to achieve the engine thrust, (9) further obtains as

$$\dot{V}_i = \frac{\boldsymbol{v}_i^{\mathrm{T}}}{V_i}\left(R_1^{\mathrm{T}}(\boldsymbol{\varphi}_i)\boldsymbol{g} + \frac{F_{a_i}}{m_i} + \boldsymbol{d}_{v_i}\right) + \frac{u_iF_{Txi}}{m_iV_i}, \tag{10}$$

where $\boldsymbol{v}_i^{\mathrm{T}}S(\boldsymbol{w}_i)\boldsymbol{v}_i = 0$. Similarly, the aerodynamic force $\boldsymbol{F}_{a_i}$ is decomposed into known term $\boldsymbol{F}_{a_{i0}}$ and uncertain term $\Delta\boldsymbol{F}_{a_i}$, and the engine failure is considered as:

$$F_{Txi} = \varrho_{Ti}F_{Txi0} + F_{Txif}, \tag{11}$$

where F_{Txi0} is the desired thrust, $\varrho_{Ti} \in [0,1]$ is the unknown effectiveness factor of the thrust and F_{Txif} is unknown bias fault. The term ϱ_{Ti} represents the efficiency factor of the actuators with three cases: (i) *Normal Condition*: $\varrho_{Ti} = 1, F_{Txif} = 0$; (ii) *Efficiency Loss*: $\varrho_{Ti} \in (0,1), F_{Txif} = 0$; (iii) *Bias fault*: $\varrho_{Ti} = 1, F_{Txif} \neq 0$.

Consequently, the temporal evolution of the scalar speed V_i is derived as follows:

$$\dot{V}_i = \frac{u_i\varrho_{Ti}F_{Txi0}}{m_iV_i} + \frac{\boldsymbol{v}_i^{\mathrm{T}}}{V_i}\left(\boldsymbol{R}_1^{\mathrm{T}}(\boldsymbol{\varphi}_i)\boldsymbol{g} + \frac{\boldsymbol{F}_{a_{i0}}}{m_i} + \frac{\Delta\boldsymbol{F}_{a_i}}{m_i} + \boldsymbol{d}_{v_i}\right) + \frac{u_iF_{Txif}}{m_iV_i}. \tag{12}$$

Furthermore, we can simplify the speed dynamics into the following compact form:

$$\dot{V}_i = f_{vi} + g_{vi}F_{Txi0} + D_{Vi} \tag{13}$$

where $f_{vi} = \frac{\boldsymbol{v}_i^{\mathrm{T}}}{V_i}(\boldsymbol{R}_1^{\mathrm{T}}\boldsymbol{g} + \frac{\boldsymbol{F}_{ai0}}{m_i})$, $g_{vi} = \frac{u_i}{m_iV_i}$, and $D_{Vi} = \frac{u_i}{m_iV_i}[(\kappa_{Ti} - 1)F_{Txi0} + F_{Txif}] + \frac{\boldsymbol{v}_i^{\mathrm{T}}}{V_i}(\frac{\Delta\boldsymbol{F}_{a_{i0}}}{m_i} + \boldsymbol{d}_{vi})$ is the lumped disturbance.

Utilizing the identical analytical procedure, the rotational dynamics of the lead-UAV (UAV 0) are structured in state-space form:

$$\begin{bmatrix} \dot{\boldsymbol{X}}_{01} \\ \dot{\boldsymbol{X}}_{02} \end{bmatrix} = \begin{bmatrix} \mathbf{0}_{3\times3} & \boldsymbol{I}_3 \\ \mathbf{0}_{3\times3} & \mathbf{0}_{3\times3} \end{bmatrix} \begin{bmatrix} \boldsymbol{X}_{01} \\ \boldsymbol{X}_{02} \end{bmatrix} + \begin{bmatrix} \mathbf{0}_{3\times3} \\ \boldsymbol{G}_0(\boldsymbol{X}_0) \end{bmatrix}, \tag{14}$$

while the corresponding translational motion is governed by $\dot{\boldsymbol{X}}_{03} = \boldsymbol{F}_0(\boldsymbol{X}_0)$, where $\boldsymbol{X}_{01} = \boldsymbol{\varphi}_0$ denotes attitude, $\boldsymbol{X}_{02} = \dot{\boldsymbol{\varphi}}_0$ is angular rate, and $\boldsymbol{X}_{03} = \boldsymbol{v}_0$ is velocity vector. The combined state vector is denoted by $\boldsymbol{X}_0 = [X_{01}^{\mathrm{T}}, X_{02}^{\mathrm{T}}, X_{03}^{\mathrm{T}}]^{\mathrm{T}}$. The nonlinear mappings $\boldsymbol{F}_0$ and $\boldsymbol{G}_0$ are expanded as: $\boldsymbol{G}_0 = (\boldsymbol{J}_0\boldsymbol{R}_2)^{-1}(\boldsymbol{F}_{b0} + \boldsymbol{C}_0\boldsymbol{\delta}_0 - \boldsymbol{S}(\boldsymbol{J}_0\boldsymbol{R}_2\dot{\boldsymbol{\varphi}}_0)\boldsymbol{R}_2\dot{\boldsymbol{\varphi}}_0 - \boldsymbol{J}_0\dot{\boldsymbol{R}}_2\dot{\boldsymbol{\varphi}}_0)$, and $\boldsymbol{F}_0 = \frac{\boldsymbol{F}_{T0}}{m_0} + \boldsymbol{R}_1^{\mathrm{T}}\boldsymbol{g} - \boldsymbol{S}(\boldsymbol{\omega}_0)\boldsymbol{v}_0 + \frac{\boldsymbol{F}_{a0}}{m_0}$.

2.3. Lemma and Assumption

Definition 1 ([37]). *Let us investigate the class of nonlinear uncertain systems $\dot{\boldsymbol{x}} = \boldsymbol{f}(t, \boldsymbol{x}), \boldsymbol{x}(0) = \boldsymbol{x}_0$, with state vector $\boldsymbol{x} \in \mathbb{R}^n$ and a continuous nonlinear mapping $\boldsymbol{f} : \mathbb{R}^+ \times \mathbb{R}^n \to \mathbb{R}^n$. The equilibrium point of this system is categorized as prescribed-time stable if the states converge to the origin within a prescribed duration $T(\boldsymbol{x}_0)$ that is upper-bounded by a user-defined constant $T_{\max}$, regardless of the initial condition $\boldsymbol{x}_0 \in \mathbb{R}^n$. Furthermore, define the system as practical prescribed-time stable if for any given $T \in \mathbb{R}^+$, there exists a small neighborhood ϖ such that $\|\boldsymbol{x}(t; \boldsymbol{x}_0)\| \leq \varpi$ holds for all $t \geq T$.*

Assumption 1. *Within the 6-DOF framework, all parameter uncertainties and external environmental disturbances are assumed to be constrained within specific bounds, satisfying: $\|\boldsymbol{d}_{\omega_i}\| \leq \bar{d}_{\omega_i}$, $\|\boldsymbol{B}_{i3}\| \leq \bar{\boldsymbol{B}}_{i3}$, $\|\boldsymbol{\Delta}_{v_i}\| \leq \bar{\Delta}_{v_i}$, $\|\boldsymbol{\delta}_{if}\| \leq \bar{\delta}_{if}$, $|F_{Txif}| \leq \bar{F}_{Txif}$, and $\|\boldsymbol{d}_{v_i}\| \leq \bar{d}_{v_i}$.*

Assumption 2. *Regarding the leader aircraft, the nonlinear functions $\boldsymbol{G}_0$ and $\boldsymbol{F}_0$ are assumed to satisfy the localized Lipschitz condition with respect to their arguments, such that: $\|\boldsymbol{F}_0(\boldsymbol{X}_0) - \boldsymbol{F}_0(\boldsymbol{Y}_0)\| \leq \gamma_1\|\boldsymbol{X}_0 - \boldsymbol{Y}_0\|$, $\|\boldsymbol{G}_0(\boldsymbol{X}_0) - \boldsymbol{G}_0(\boldsymbol{Y}_0)\| \leq \gamma_2\|\boldsymbol{X}_0 - \boldsymbol{Y}_0\|$.*

Assumption 3. *The temporal variation of the total disturbance $\boldsymbol{D}$ is assumed to be constrained, such that its derivative satisfies $\|\dot{\boldsymbol{D}}(t)\| \leq M$, where M is a positive, albeit unknown, scalar.*

Lemma 1 ([31]). *Consider a differentiable Reference Convergence Function (RCF), denoted as $\zeta(z)$, which satisfies the following differential relationship:*

$$\dot{\zeta}(z) = -\frac{\eta\beta(\zeta(z))\,\mathrm{arc}(\zeta(z))}{T - t} = -\kappa(\zeta(z), t) \tag{15}$$

with $z = (T - t)^\eta$ and $\eta > 1$. The RCF $\zeta(z)$ and its associated derivative function $\kappa(\zeta(z), t)$ possess the subsequent properties: (i) At the terminal time $t = T$, both $\zeta(z)$ and $\kappa(\zeta(z), t)$ vanish (i.e., equal to zero). (ii) On $[0, T]$, $\zeta(z)$ maintains continuity and monotonic behavior, where T signifies the pre-assigned settling time. (iii) Asymptotic behavior is exhibited as $z \to 0$ satisfies $\zeta(z) \sim z$ and $\lim_{z\to0}[\zeta(z)/z] = 1$. (iv) The terms are related via $\mathrm{arc}[\zeta(z)] = z$ and $\beta[\zeta(z)] = \partial x/\partial y$.

Lemma 2. *The mapping $h(x) = (1 + x^2)\arctan(x)$ is established as a convex function.*

Lemma 3 ([38]). *Define a convex function $f(x)$, and a set of weights p_i such that $\sum_{i=1}^m p_i = 1$; then the following inequality holds:*

$$\sum_{i=1}^{m} p_i h(x_i) \leq h\left(\sum_{i=1}^{m} p_i x_i\right), \quad \forall x_i \in I. \tag{16}$$

In the specific case where $p_i = 1/m$ for all i, this simplifies to:

$$\frac{1}{m}\sum_{i=1}^{m} f(x_i) \leq f\left(\frac{1}{m}\sum_{i=1}^{m} x_i\right). \tag{17}$$

Control Objective: The primary goal of this study is to design a control law to achieve high-precision formation tracking control for fixed-wing UAVs within a prescribed time, ensuring robustness against actuator faults and external disturbance throughout the entire operational duration. Figure 2 depicts the overall architecture of learning-based safety control design.

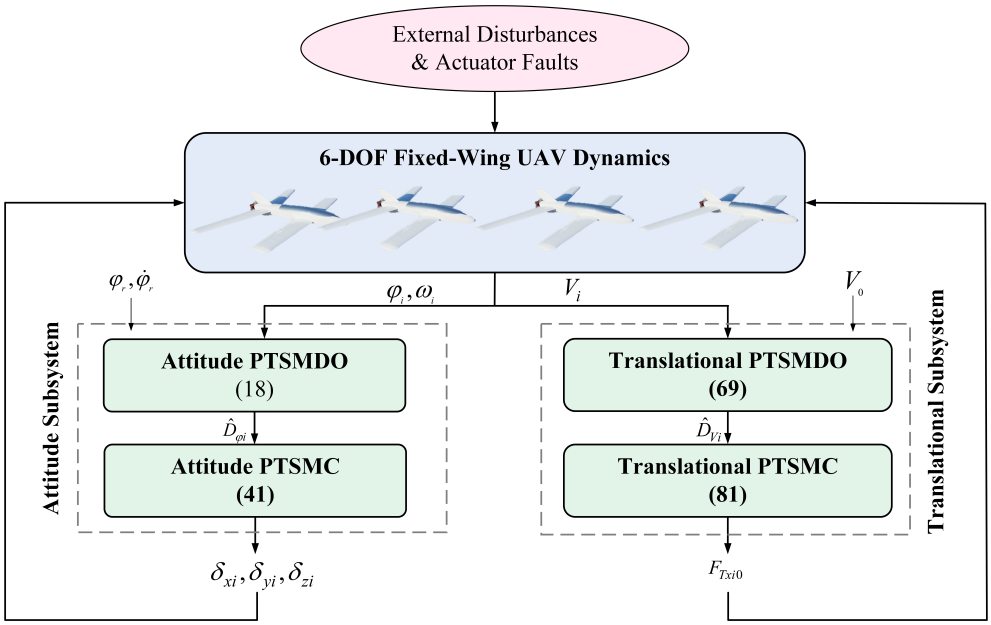


Figure 2. Overall architecture of the learning-based safety control scheme.

3. Prescribed-Time Formation Tracking Control Strategy with Sliding Mode Disturbance Observer

3.1. Attitude Control via Prescribed-Time Sliding Mode Control Strategy

Define the tracking errors for the attitude subsystem as follows:

$$\boldsymbol{e}_{i1} = \boldsymbol{\varphi}_i - \boldsymbol{\varphi}_r, \quad \boldsymbol{e}_{i2} = \boldsymbol{M}_i - \dot{\boldsymbol{\varphi}}_r \tag{18}$$

where $\boldsymbol{\varphi}_r = [\phi_r, \theta_r, \psi_r]^{\mathrm{T}}$ signifies the reference trajectory. The vectors $\boldsymbol{e}_{\varphi i1} = [e^1_{\varphi i1}, e^2_{\varphi i1}, e^3_{\varphi i1}]^{\mathrm{T}}$ and $\boldsymbol{e}_{\varphi i2} = [e^1_{\varphi i2}, e^2_{\varphi i2}, e^3_{\varphi i2}]^{\mathrm{T}}$ represent the tracking error.

By integrating the kinematics and dynamics from (8), the error dynamics are:

$$\begin{cases} \dot{\boldsymbol{e}}_{\varphi i1} = \boldsymbol{e}_{\varphi i2} \\ \dot{\boldsymbol{e}}_{\varphi i2} = \boldsymbol{B}_{i1}\boldsymbol{\delta}_{i0} + \boldsymbol{D}_{\varphi i} - \ddot{\boldsymbol{\varphi}}_r \end{cases} \tag{19}$$

3.1.1. Prescribed-Time Sliding Mode Disturbance Observer

A primary challenge in the error model is the requirement for precise knowledge of the total disturbance $\boldsymbol{D}_{\varphi i}$, which is typically inaccessible in practical flight. To circumvent this, we propose a prescribed-time observer to estimate the uncertain term $\boldsymbol{D}_{\varphi i}$. An auxiliary state variable $\boldsymbol{\vartheta}_{\varphi i} = [\vartheta_{\varphi i1}, \vartheta_{\varphi i2}, \vartheta_{\varphi i3}]^{\mathrm{T}} \in \mathbb{R}^3$ is formulated:

$$\boldsymbol{\vartheta}_{\varphi i} = -\boldsymbol{\kappa}_{\varphi i1}\int_0^{\mathrm{T}} (\boldsymbol{B}_{i1}\boldsymbol{\delta}_{i0} + \boldsymbol{\kappa}_{\varphi i2}\boldsymbol{\vartheta}_{\varphi i})d\nu + \boldsymbol{\kappa}_{\varphi i1}\boldsymbol{M}_i \tag{20}$$

where the positive definite matrices are denoted by $\boldsymbol{\kappa}_{\varphi i1} = \mathrm{diag}[\kappa^1_{\varphi i1}, \kappa^2_{\varphi i1}, \kappa^3_{\varphi i1}]$ and $\boldsymbol{\kappa}_{\varphi i2} = \mathrm{diag}[\kappa^1_{\varphi i2}, \kappa^2_{\varphi i2}, \kappa^3_{\varphi i2}]$. By differentiating $\boldsymbol{\vartheta}_{\varphi i}$ with respect to time, it can be shown that this new state acts as a first-order filter for the lumped disturbance with $\dot{\boldsymbol{\vartheta}}_{\varphi i} = -\boldsymbol{\kappa}_{\varphi i1}\boldsymbol{\kappa}_{\varphi i2}\boldsymbol{\vartheta}_i + \boldsymbol{\kappa}_{\varphi i1}\boldsymbol{D}_{\varphi i}$.

Let $\hat{\boldsymbol{\vartheta}}_{\varphi i}$ be the estimate of $\boldsymbol{\vartheta}_{\varphi i}$, and define the estimation discrepancy as $\boldsymbol{z}_{\varphi i0} = \boldsymbol{\vartheta}_{\varphi i} - \hat{\boldsymbol{\vartheta}}_{\varphi i} \in \mathbb{R}^3$. Subsequently, we introduce an integral sliding surface $\boldsymbol{z}_{\varphi i1}$ such that:

$$\boldsymbol{z}_{\varphi i1} = \boldsymbol{z}_{\varphi i0} + \int_0^{\mathrm{T}} \boldsymbol{\zeta}_{\varphi i0} d\nu \tag{21}$$

where $\boldsymbol{\zeta}_{\varphi i0} = \mathrm{diag}[\zeta^1_{\varphi i0}, \zeta^2_{\varphi i0}, \zeta^3_{\varphi i0}]$ and $\boldsymbol{z}_{\varphi i1} = [z^1_{\varphi i1}, z^2_{\varphi i1}, z^3_{\varphi i1}]^{\mathrm{T}}$.

Theorem 1. *For the UAV attitude dynamics subject to compound disturbances, consider the observer architecture designed as:*

$$\begin{cases} \dot{\hat{\boldsymbol{\vartheta}}}_{\varphi i} = \dot{\boldsymbol{\vartheta}}_{\varphi i} + \boldsymbol{\zeta}_{\varphi i0} + \boldsymbol{\zeta}_{\varphi i1} \\ \hat{\boldsymbol{D}}_{\varphi i} = \boldsymbol{\kappa}_{\varphi i2}\hat{\boldsymbol{\vartheta}}_{\varphi i} + \boldsymbol{\kappa}^{-1}_{\varphi i1}\dot{\boldsymbol{\vartheta}}_{\varphi i} \end{cases} \tag{22}$$

where $\hat{\boldsymbol{D}}_{\varphi i}$ signifies the estimated value of $\boldsymbol{D}_{\varphi i}$. The gains $\boldsymbol{\zeta}_{\varphi i1} = \mathrm{diag}[\zeta^1_{\varphi i1}, \zeta^2_{\varphi i1}, \zeta^3_{\varphi i1}]$ are configured as:

$$\zeta^p_{\varphi i0} = \begin{cases} \dfrac{k^p_{\varphi i1}(1+(z_{\varphi i0})^2)\arctan(z^p_{\varphi i0})}{T_{d_{\varphi i0}} - t + k^p_{\varphi i3}} & 0 \le t < T_{d_{\varphi i0}} \\ \left[\exp\left(\dfrac{\sqrt{k^p_{\varphi i2}}}{k^p_{\varphi i3}} - \dfrac{k^p_{\varphi i2}}{t - T_{d_{\varphi i0}} + \sqrt{k^p_{\varphi i2}}k^p_{\varphi i3}}\right) + \dfrac{k^p_{\varphi i1}}{k^p_{\varphi i3}} - 1\right] z^p_{\varphi i0} & t \ge T_{d_{\varphi i0}} \end{cases} \tag{23}$$

$$\zeta^p_{\varphi i1} = \begin{cases} \dfrac{k^p_{\varphi i4}(1+(z_{\varphi i1})^2)\arctan(z^p_{\varphi i1})}{T_{d_{\varphi i1}} - t + k^p_{\varphi i6}} & 0 \le t < T_{d_{\varphi i1}} \\ \left[\exp\left(\dfrac{\sqrt{k^p_{\varphi i5}}}{k^p_{\varphi i6}} - \dfrac{k^p_{\varphi i5}}{t - T_{d_{\varphi i1}} + \sqrt{k^p_{\varphi i5}}k^p_{\varphi i6}}\right) + \dfrac{k^p_{\varphi i4}}{k^p_{\varphi i6}} - 1\right] z^p_{\varphi i1} & t \ge T_{d_{\varphi i1}} \end{cases} \tag{24}$$

where $p \in \{1, 2, 3\}$, and the parameters $k^p_{\varphi i1}, \ldots, k^p_{\varphi i6}$ are strictly positive constants satisfying $k^p_{\varphi i1} > k^p_{\varphi i3}$ and $k^p_{\varphi i4} > k^p_{\varphi i6}$. Under these conditions, the estimation of the lumped disturbance $\boldsymbol{D}_{\varphi i}$ is achieved precisely within the pre-specified time.

Proof of Theorem 1. Utilizing (24), the dynamics of the sliding variable can be described by $\dot{\boldsymbol{z}}_{\varphi i1} = -\boldsymbol{\zeta}_{\varphi i1}$. To evaluate the stability of this observer, we select a Lyapunov candidate $L_{z_{\varphi i1}} = \frac{1}{2}\boldsymbol{z}^{\mathrm{T}}_{\varphi i1}\boldsymbol{z}_{\varphi i1}$. The analysis is conducted across two cases:

Case 1: For $t \in [0, T_{d_{\varphi i1}})$, the derivative of the Lyapunov function yields:

$$\dot{L}_{z_{\varphi i1}} = -\boldsymbol{\zeta}_{\varphi i1}\boldsymbol{z}_{\varphi i1} = -\sum_{i=1}^{3} \frac{k^p_{\varphi i4}|z^p_{\varphi i1}|(1 + (z^p_{\varphi i1})^2)\arctan(|z^p_{\varphi i1}|)}{T_{d_{\varphi i1}} - t + k^p_{\varphi i6}} \tag{25}$$

By defining the auxiliary mapping $\varepsilon(z^p_{\varphi i1}) = (1 + (z^p_{\varphi i1})^2)\arctan(|z^p_{\varphi i1}|)$ and invoking **Lemma 1** and **Lemma 3**, we can bound the derivative as:

$$\begin{aligned} \dot{L}_{z_{\varphi i1}} &\le -\frac{3\min\{k^1_{\varphi i4}, k^2_{\varphi i4}, k^3_{\varphi i4}\}\|\boldsymbol{z}_{\varphi i1}\|_1}{3}\varepsilon\left(\frac{\|\boldsymbol{z}_{\varphi i1}\|_1}{3}\right) \cdot \frac{1}{T_{d_{\varphi i1}} - t + \max\{k^1_{\varphi i6}, k^2_{\varphi i6}, k^3_{\varphi i6}\}} \\ &\le -\frac{3\min\{k^1_{\varphi i4}, k^2_{\varphi i4}, k^3_{\varphi i4}\}\sqrt{L_{z_{\varphi i1}}}}{3}\varepsilon\left(\frac{\sqrt{L_{z_{\varphi i1}}}}{3}\right) \cdot \frac{1}{T_{d_{\varphi i1}} - t + \max\{k^1_{\varphi i6}, k^2_{\varphi i6}, k^3_{\varphi i6}\}} \end{aligned} \tag{26}$$

Let $m_{\varphi i1} = \sqrt{L_{z_{\varphi i1}}}/3$. It is described by $\dot{m}_{\varphi i1} = \frac{\dot{L}_{z_{\varphi i1}}}{6\sqrt{L_{z_{\varphi i1}}}} \leq -\frac{\min\{k^1_{\varphi i4}, k^2_{\varphi i4}, k^3_{\varphi i4}\}\varepsilon(m_{\varphi i1})}{6(T_{d_{\varphi i1}} - t + \max\{k^1_{\varphi i6}, k^2_{\varphi i6}, k^3_{\varphi i6}\})}$. Further, one has:

$$\begin{aligned}\dot{m}_{\varphi i1} &\leq -\frac{\min\{k^1_{\varphi i4}, k^2_{\varphi i4}, k^3_{\varphi i4}\}(1 + m^2_{\varphi i1})\arctan(m_{\varphi i1})}{6\left(T_{d_{\varphi i1}} - t + \max\{k^1_{\varphi i6}, k^2_{\varphi i6}, k^3_{\varphi i6}\}\right)} \\ &\leq -\frac{\min\{k^1_{\varphi i4}, k^2_{\varphi i4}, k^3_{\varphi i4}\}}{6\left(T_{d_{\varphi i1}} - t + \max\{k^1_{\varphi i6}, k^2_{\varphi i6}, k^3_{\varphi i6}\}\right)} m_{\varphi i1}\end{aligned} \tag{27}$$

Solving this inequality leads to:

$$\begin{aligned}m_{\varphi i1} &\leq m_{\varphi i1}(0) e^{\int_0^t -\frac{\min\{k^1_{\varphi i4}, k^2_{\varphi i4}, k^3_{\varphi i4}\}}{6\left(T_{d_{\varphi i1}} - t + \max\{k^1_{\varphi i6}, k^2_{\varphi i6}, k^3_{\varphi i6}\}\right)} ds} \\ &= m_{\varphi i1}(0)\left(\frac{T_{d_{\varphi i1}} - t + \max\{k^1_{\varphi i6}, k^2_{\varphi i6}, k^3_{\varphi i6}\}}{T_{d_{\varphi i1}} + \max\{k^1_{\varphi i6}, k^2_{\varphi i6}, k^3_{\varphi i6}\}}\right)^{\frac{\min\{k^1_{\varphi i4}, k^2_{\varphi i4}, k^3_{\varphi i4}\}}{6}}\end{aligned} \tag{28}$$

This means that by selecting a suitable parameter, $m_{\varphi i1}$, as well as $L_{z_{\varphi i1}}$, it can converge to a small domain before $t = T_{d_{\varphi i1}}$; thus, one has that $z_{\varphi i1}$ converge on $t \leq T_{d_{\varphi i1}}$. Another inequality of $L_{z_{\varphi i1}}$ can be expressed as

$$\begin{aligned}\dot{L}_{z_{\varphi i1}} = -\boldsymbol{\zeta}_{\varphi i1}\boldsymbol{z}_{\varphi i1} &\geq -\frac{(k^1_{\varphi i4} + k^2_{\varphi i4} + k^3_{\varphi i4})\|z_{\varphi i1}\|_\infty \varepsilon(\|z_{\varphi i1}\|_\infty)}{T_{d_{\varphi i1}} - t + \min\{k^1_{\varphi i6}, k^2_{\varphi i6}, k^3_{\varphi i6}\}} \\ &\geq -\frac{(k^1_{\varphi i4} + k^2_{\varphi i4} + k^3_{\varphi i4})\sqrt{L_{z_{\varphi i1}}}\varepsilon(\sqrt{L_{z_{\varphi i1}}})}{T_{d_{\varphi i1}} - t + \min\{k^1_{\varphi i6}, k^2_{\varphi i6}, k^3_{\varphi i6}\}}\end{aligned} \tag{29}$$

Let $m_{\varphi i2} = \sqrt{L_{z_{\varphi i1}}}$, and its derivative is $\dot{m}_{\varphi i2} = -\frac{\dot{L}_{z_{\varphi i1}}}{2\sqrt{L_{z_{\varphi i1}}}} \geq -\frac{(k^1_{\varphi i4} + k^2_{\varphi i4} + k^3_{\varphi i4})\varepsilon(m_{\varphi i2})}{2(T_{d_{\varphi i1}} - t + \min\{k^1_{\varphi i6}, k^2_{\varphi i6}, k^3_{\varphi i6}\})}$. Following the properties of Gronwall's inequality and the results in [31], it is concluded that $L_{z_{\varphi i1}}$ converges. Combined with the previous analysis and applying the squeeze theorem, we confirm that $z_{\varphi i1}$ reaches a neighborhood near zero.

Case 2: For $t \in [T_{d_{\varphi i1}}, \infty)$, the following equation can be satisfied:

$$\begin{aligned}\dot{L}_{z_{\varphi i1}} &= -\sum_{i=1}^{3}\left[\exp\left(\frac{\sqrt{k^p_{\varphi i5}}}{k^p_{\varphi i6}} - \frac{k^p_{\varphi i5}}{t - T_{d_{\varphi i1}} + \sqrt{k^p_{\varphi i5}}k^p_{\varphi i6}}\right) + \frac{k^p_{\varphi i4}}{k^p_{\varphi i6}} - 1\right] z^2_{\varphi i1} \\ &\leq -2L_{z_{\varphi i1}} min\left\{\exp\left(\frac{\sqrt{k^1_{\varphi i5}}}{k^1_{\varphi i6}} - \frac{k^1_{\varphi i5}}{t - T_{d_{\varphi i1}} + \sqrt{k^1_{\varphi i5}}k^1_{\varphi i6}}\right) + \frac{k^1_{\varphi i4}}{k^1_{\varphi i6}} - 1,\right. \\ &\quad \exp\left(\frac{\sqrt{k^2_{\varphi i5}}}{k^2_{\varphi i6}} - \frac{k^2_{\varphi i5}}{t - T_{d_{\varphi i1}} + \sqrt{k^2_{\varphi i5}}k^2_{\varphi i6}}\right) + \frac{k^2_{\varphi i4}}{k^2_{\varphi i6}} - 1, \\ &\quad \left.\exp\left(\frac{\sqrt{k^3_{\varphi i5}}}{k^3_{\varphi i6}} - \frac{k^3_{\varphi i5}}{t - T_{d_{\varphi i1}} + \sqrt{k^3_{\varphi i5}}k^3_{\varphi i6}}\right) + \frac{k^3_{\varphi i5}}{k^3_{\varphi i6}} - 1\right\} \\ &\leq -2\left(\exp\left(\frac{\sqrt{k'_{\varphi i5}}}{k'_{\varphi i6}} - \frac{k'_{\varphi i5}}{t - T_{d_{\varphi i1}} + \sqrt{k'_{\varphi i5}}k'_{\varphi i6}}\right) + \frac{k'_{\varphi i4}}{k'_{\varphi i6}} - 1\right) L_{z_{\varphi i1}}\end{aligned} \tag{30}$$

where $\boldsymbol{k}'_{\varphi 4} = \min\{k^1_{\varphi i4}, k^2_{\varphi i4}, k^3_{\varphi i4}\}$, $\boldsymbol{k}'_{\varphi i6} = \max\{k^1_{\varphi i6}, k^2_{\varphi i6}, k^3_{\varphi i6}\}$, $\boldsymbol{k}'_{\varphi 5} = \min\{k^1_{\varphi i5}, k^2_{\varphi i5}, k^3_{\varphi i5}\}$.

Through the application of Gronwall's lemma, it follows that:

$$\begin{aligned} L_{z_{\varphi i1}} &\leq L_{z_{\varphi i1}}(0) e^{\int_{T_{d_{\varphi i1}}}^{t} -2\left[\exp\left(\frac{\sqrt{k'_{\varphi i5}}}{k'_{\varphi i6}} - \frac{k'_{\varphi i5}}{z_{\varphi i0} - T_{d_{\varphi i1}} + \sqrt{k'_{\varphi i5}} k'_{\varphi i6}}\right) + \frac{k'_{\varphi i4}}{k'_{\varphi i6}} - 1\right] ds} \\ &= L_{z_{\varphi i1}}(0) e^{-2\int_{T_{d_{\varphi i1}}}^{t} \exp\left(\frac{\sqrt{k'_{\varphi i5}}}{k'_{\varphi i6}} - \frac{k'_{\varphi i5}}{z_{\varphi i0} - T_{d_{\varphi i1}} + \sqrt{k'_{\varphi i5}} k'_{\varphi i6}}\right) ds} e^{-2\left(\frac{k'_{\varphi i4}}{k'_{\varphi i6}} - 1\right)(t - T_{d_{\varphi i1}})} \end{aligned} \tag{31}$$

Hence, by tuning the observer parameters, the estimation error remains bounded within a negligible region following the specified time.

A similar Lyapunov analysis can be applied to $L_{z_{\varphi i2}} = \frac{1}{2} \boldsymbol{z}^{\mathrm{T}}_{\varphi i0} \boldsymbol{z}_{\varphi i0}$, demonstrating that $\dot{\boldsymbol{z}}_{\varphi i0} = -\boldsymbol{\zeta}_{\varphi i0}$ ensures prescribed-time convergence.

Case 1: For $t \in [0, T_{z_{\varphi i0}})$, the following relation is established:

$$\dot{L}_{z_{\varphi i2}} = -\boldsymbol{\zeta}^{\mathrm{T}}_{\varphi i0} \boldsymbol{z}_{i0} = -\sum_{i=1}^{3} \frac{k^p_{\varphi i1} |z^p_{\varphi i0}| (1 + (z^p_{\varphi i0})^2) \arctan(|z_{\varphi i0}|^p)}{T_{z_{\varphi i0}} - t + k^p_{\varphi i3}} \tag{32}$$

Let us define the auxiliary function $\varepsilon(z_{\varphi i0}) = (1 + z^2_{\varphi i0}) \arctan(|z_{\varphi i0}|)$. Based on the properties established in **Lemma 1** and **Lemma 3**, the temporal derivative of $L_{z_{\varphi i2}}$ can be bounded as:

$$\begin{aligned} \dot{L}_{z_{\varphi i2}} &\leq -\frac{3 \min\{k^1_{\varphi i1}, k^2_{\varphi i1}, k^3_{\varphi i1}\} \frac{\|z_{\varphi i0}\|_1}{3} \varepsilon\left(\frac{\|z_{\varphi i0}\|_1}{3}\right)}{T_{z_{\varphi i0}} - t + k'_{\varphi i3}} \\ &\leq -\frac{3 \min\{k^1_{\varphi i1}, k^2_{\varphi i1}, k^3_{\varphi i1}\} \frac{\sqrt{L_{z_{\varphi i2}}}}{3} \varepsilon\left(\frac{\sqrt{L_{z_{\varphi i2}}}}{3}\right)}{T_{z_{\varphi i0}} - t + k'_{\varphi i3}} \end{aligned} \tag{33}$$

where $k'_{\varphi i3} = \max\{k^1_{\varphi i3}, k^2_{\varphi i3}, k^3_{\varphi i3}\}$. We now introduce the auxiliary variable $m_{i3} = \frac{\sqrt{L_{z_{\varphi i2}}}}{3}$. Its derivative satisfies the following inequality $m_{i3} = \frac{\dot{L}_{z_{\varphi i2}}}{6\sqrt{L_{z_{\varphi i2}}}} \leq -\frac{\min\{k^1_{\varphi i1}, k^2_{\varphi i1}, k^3_{\varphi i1}\} \varepsilon(m_{i3})}{6(T_{z_{\varphi i0}} - t + k'_{\varphi i3})}$. Furthermore, it follows that:

$$\dot{m}_{i3} \leq -\frac{\min\{k^1_{\varphi i1}, k^2_{\varphi i1}, k^3_{\varphi i1}\}(1 + m^2_{i3}) \arctan(m_{i3})}{6(T_{z_{\varphi i0}} - t + k'_{\varphi i3})} \leq -\frac{\min\{k^1_{\varphi i1}, k^2_{\varphi i1}, k^3_{\varphi i1}\} m_{i3}}{6(T_{z_{\varphi i0}} - t + k'_{\varphi i3})} \tag{34}$$

By integrating both sides, we obtain:

$$m_{i3} \leq m_{i3}(0) e^{\int_0^{T_{z_{\varphi i0}}} \frac{-\min\{k^1_{\varphi i1}, k^2_{\varphi i1}, k^3_{\varphi i1}\}}{6(T_{z_{\varphi i0}} - s + k'_{\varphi i3})} ds} = m_{i3}(0) \left(\frac{T_{z_{\varphi i0}} - t + k'_{\varphi i3}}{T_{z_{\varphi i0}} + k'_{\varphi i3}}\right)^{\frac{\min\{k^1_{\varphi i1}, k^2_{\varphi i1}, k^3_{\varphi i1}\}}{6}} \tag{35}$$

The result above demonstrates that through a proper configuration of parameters, both m_{i3} and $L_{z_{\varphi i2}}$ are capable of converging prior to the time $t = T_{z_{\varphi i0}} + k_{\varphi i3}$. Consequently, the error vector $\boldsymbol{z}_{\varphi i0}$ is guaranteed to enter a compact neighborhood within $t \leq T_{z_{\varphi i0}} + k_{\varphi i3}$.

Additionally, another bound for the trajectory of $L_{z_{\varphi i2}}$ is expressed as:

$$\begin{aligned}\dot{L}_{z_{\varphi i2}} = -\boldsymbol{\zeta}_{\varphi i0}\boldsymbol{z}_{i0} &\geq -\frac{(k^1_{\varphi i1}+k^2_{\varphi i1}+k^3_{\varphi i1})\|z_{\varphi i0}\|_\infty \varepsilon(\|z_{\varphi i0}\|_\infty)}{T_{d_{\varphi i1}}-t+\min\{k^1_{\varphi i3},k^2_{\varphi i3},k^3_{\varphi i3}\}} \\ &\geq -\frac{(k^1_{\varphi i1}+k^2_{\varphi i1}+k^3_{\varphi i1})\sqrt{L_{z_{\varphi i2}}}\varepsilon(\sqrt{L_{z_{\varphi i2}}})}{T_{d_{\varphi i1}}-t+\min\{k^1_{\varphi i3},k^2_{\varphi i3},k^3_{\varphi i3}\}}\end{aligned} \tag{36}$$

Letting $m_{i4} = \sqrt{L_{z_{\varphi i2}}}$, the corresponding derivative is given by $\dot{m}_{i4} = -\frac{\dot{L}_{z_{\varphi i2}}}{2\sqrt{L_{z_{\varphi i2}}}} \geq -\frac{(k_{\varphi i1}+k^2_{\varphi i1}+k^3_{\varphi i1})(1+m^2_{i4})\arctan(|m_{i4}|)}{2(T_{z_{\varphi i0}}-t+\min\{k^1_{\varphi i3},k^2_{\varphi i3},k^3_{\varphi i3}\})}$. This implies that the convergence of $m_{\varphi i2}$ and $L_{z_{\varphi i1}}$ is achieved after. By invoking the squeeze theorem, we conclude that the state $z_{\varphi i1}$ converges exactly at the prescribed moment.

Case 2: For $t \in [T_{z_{\varphi i0}}, \infty)$, the system satisfies the following dynamics:

$$\begin{aligned}\dot{L}_{z_{\varphi i2}} &= -\sum_{p=1}^{3}\left[\exp\left(\frac{\sqrt{k^p_{\varphi i2}}}{k^p_{\varphi i3}}-\frac{k^p_{\varphi i2}}{t-T_{z_{\varphi i0}}+\sqrt{k^p_{\varphi i2}}k^p_{\varphi i1}}\right)+\frac{k^p_{\varphi i1}}{k^p_{\varphi i3}}-1\right]z^2_{\varphi i0} \\ &\leq -2L_{z_{\varphi i2}}\min\left\{\exp\left(\frac{\sqrt{k^1_{\varphi i2}}}{k^1_{\varphi i3}}-\frac{k^1_{\varphi i2}}{t-T_{z_{\varphi i0}}+\sqrt{k^1_{\varphi i2}}k^1_{\varphi i1}}\right)+\frac{k^1_{\varphi i1}}{k^1_{\varphi i3}}-1,\right. \\ &\qquad \exp\left(\frac{\sqrt{k^2_{\varphi i2}}}{k^2_{\varphi i3}}-\frac{k^2_{\varphi i2}}{t-T_{z_{\varphi i0}}+\sqrt{k^2_{\varphi i2}}k^2_{\varphi i3}}\right)+\frac{k^2_{\varphi i1}}{k^2_{\varphi i3}}-1, \\ &\qquad \left.\exp\left(\frac{\sqrt{k^3_{\varphi i2}}}{k^3_{\varphi i3}}-\frac{k^3_{\varphi i2}}{t-T_{z_{\varphi i0}}+\sqrt{k^3_{\varphi i2}}k^3_{\varphi i3}}\right)+\frac{k^3_{\varphi i1}}{k^3_{\varphi i3}}-1\right\} \\ &\leq -2\left(\exp\left(\frac{\sqrt{k'_{i2}}}{k'_{i3}}-\frac{k'_{i2}}{t-T_{z_{\varphi i0}}+\sqrt{k'_{i2}}k'_{i3}}\right)+\frac{k'_{i1}}{k'_{i3}}-1\right)L_{z_{\varphi i2}}\end{aligned} \tag{37}$$

where the lumped coefficients are defined as $\boldsymbol{k}'_{\varphi 4} = \min\{k^1_{\varphi i4},k^2_{\varphi i4},k^3_{\varphi i4}\}$, $\boldsymbol{k}'_{\varphi i6} = \max\{k^p_{\varphi 61},k^p_{\varphi 62},k^p_{\varphi 63}\}$, and $\boldsymbol{k}'_{\varphi 5} = \min\{k^p_{\varphi 51},k^p_{\varphi 52},k^p_{\varphi 53}\}$.

Applying Gronwall's lemma, the following inequality is obtained:

$$\begin{aligned}L_{z_{\varphi i2}} &\leq L_{z_{\varphi i2}}(0)e^{\int_{T_{z_{\varphi i0}}}^{t}-2\left(\exp\left(\frac{\sqrt{k'_{\varphi i2}}}{k'_{\varphi i3}}-\frac{k'_{\varphi i2}}{s_i-T_{d_{\varphi i0}}+\sqrt{k'_{\varphi i2}}k'_{\varphi i1}}\right)+\frac{k'_{\varphi i1}}{k'_{\varphi i3}}-1\right)ds} \\ &= L_{z_{\varphi i2}}(0)e^{-2\int_{T_{z_{\varphi i0}}}^{t}\exp\left(\frac{\sqrt{k'_{\varphi i2}}}{k'_{\varphi i3}}-\frac{k'_{\varphi i2}}{s-T_{d_{\varphi i1}}+\sqrt{k_{\varphi i2}}k'_{\varphi i1}}\right)ds}e^{-2\left(\frac{k'_{\varphi i1}}{k'_{\varphi i3}}-1\right)(t-T_{z_{\varphi i0}})}\end{aligned} \tag{38}$$

where $\boldsymbol{k}'_{\varphi i1} = \min\{k^1_{\varphi i1},k^2_{\varphi i1},k^3_{\varphi i1}\}$, $\boldsymbol{k}'_{\varphi i2} = \min\{k^1_{\varphi i2},k^2_{\varphi i2},k^3_{\varphi i2}\}$, and $\boldsymbol{k}'_{\varphi i3} = \max\{k^1_{\varphi i3},k^2_{\varphi i3},k^3_{\varphi i3}\}$. Consequently, the estimation error is maintained within a negligible bound within the prescribed time.

From the foregoing analysis, it is evident that $z_{\varphi i0}$ achieves convergence within the specified timeframe. Defining the estimation error as $\tilde{\boldsymbol{D}}_{\varphi i} = \boldsymbol{D}_{\varphi i} - \hat{\boldsymbol{D}}_{\varphi i}$, we have:

$$\begin{aligned}\tilde{\boldsymbol{D}}_{\varphi i} &= \boldsymbol{D}_{\varphi i} - \hat{\boldsymbol{D}}_{\varphi i} = \boldsymbol{\kappa}_{\varphi i2}\boldsymbol{z}_{\varphi i0} + \boldsymbol{\kappa}^{-1}_{\varphi i1}\dot{\boldsymbol{\vartheta}}_{\varphi i} - (\boldsymbol{\kappa}_{\varphi i2}\hat{\boldsymbol{\vartheta}}_{\varphi i} + \boldsymbol{\kappa}^{-1}_{\varphi i1}\dot{\boldsymbol{\vartheta}}_{\varphi}) \\ &= \boldsymbol{\kappa}_{\varphi i2}\boldsymbol{z}_{\varphi i0}\end{aligned} \tag{39}$$

Thus, according to **Theorem 1**, $\tilde{\boldsymbol{D}}_{\varphi i}$ successfully converges to the origin, validating the performance of the proposed observer. This concludes the proof. □

Remark 1. *In the proposed PTSMDO, the upper bound of the convergence time is explicitly dictated by the predefined time parameters rather than the observer gain parameters $k_{\varphi i1}$ through $k_{\varphi i6}$. By employing a time-scale separation principle the system guarantees that full disturbance compensation is achieved prior to controller state convergence. Consequently, while the gain parameters $k_{\varphi i1}$ to $k_{\varphi i6}$ do not alter the predefined total settling time, they are instrumental in shaping the transient dynamic trajectory, regulating the initial convergence rate, and determining the ultimate steady-state precision of the disturbance estimation.*

3.1.2. Prescribed-Time Sliding Mode Control

The fundamental principle of sliding mode control involves the synthesis of a sliding manifold and a corresponding switching law. This combination is designed to compel the system's states to reach and subsequently reside on a pre-defined manifold. Specifically, the process is bifurcated into two cases: the *reaching phase*, where trajectories move from initial conditions toward the manifold, and the *sliding phase*, where they converge toward the origin along said manifold. Consequently, the SMC architecture developed here comprises two vital steps: first, the construction of a sliding variable $\boldsymbol{z}_{\varphi i}$ that encapsulates the desired control performance; and second, the derivation of a control law that ensures the manifold $\boldsymbol{z}_{\varphi i} = 0$ is reached within a finite duration from any state in the space.

To achieve stability within a strictly pre-negotiated duration, we define the following prescribed-time sliding surface: $\boldsymbol{z}_{\varphi i} = \dot{\boldsymbol{e}}_{\varphi i1} + \boldsymbol{\zeta}_{\varphi i1}$. In this formulation, the term $\boldsymbol{\zeta}_{\varphi i1} = [\zeta^1_{\varphi i1}, \zeta^2_{\varphi i1}, \zeta^3_{\varphi i1}]^{\mathrm{T}}$ is characterized by:

$$\zeta^p_{\varphi i1} = \begin{cases} \dfrac{\eta^p_{\varphi i1}(1+(e^p_{\varphi i1})^2)\arctan(e^p_{\varphi i1})}{T_{z_{\varphi i1}} - t + \delta^p_{\varphi i1}} & 0 \le t < T_{z_{\varphi i1}} \\ \left[\exp\left(\dfrac{\sqrt{\sigma^p_{\varphi i1}}}{\delta^p_{\varphi i1}} - \dfrac{\sigma^p_{\varphi i1}}{t - T_{z_{\varphi i1}} + \sqrt{\sigma^p_{\varphi i1}}\delta^p_{\varphi i1}}\right) + \dfrac{\eta^p_{\varphi i1}}{\delta^p_{\varphi i1}} - 1\right] e^p_{\varphi i1} & t \ge T_{z_{\varphi i1}} \end{cases} \tag{40}$$

where the index $p \in \{1, 2, 3\}$, and the positive scalars $\eta^p_{\varphi i1}, \sigma^p_{\varphi i1}, \delta^p_{\varphi i1}$ are design parameters. The constant $T_{z_{\varphi i1}}$ represents the allotted time for the reaching phase. Differentiating the sliding variable $\boldsymbol{z}_{\varphi i}$ with respect to time yields the following manifold dynamics:

$$\dot{\boldsymbol{z}}_{\varphi i} = \dot{\boldsymbol{e}}_{\varphi i2} + \dot{\boldsymbol{\zeta}}_{\varphi i1} \tag{41}$$

Within the SMC framework, the total control effort is partitioned into two distinct components: $\boldsymbol{\tau}_{\varphi i} = \boldsymbol{\tau}_{\varphi ie} + \boldsymbol{\tau}_{\varphi is}$. The equivalent control term $\boldsymbol{\tau}_{\varphi ie}$ is responsible for maintaining the system trajectory on the manifold once contact is established, while the switching (or reaching) component $\boldsymbol{\tau}_{\varphi is}$ is designed to drive the states toward the sliding surface from the outside. This integrated structure is essential for guaranteeing both the stability and the robustness of the closed-loop system.

Based on the error dynamics defined in (21), the equivalent controller is formulated as:

$$\boldsymbol{\tau}_{\varphi ie} = -\boldsymbol{B}^{-1}_{i1}\left(\dot{\boldsymbol{\zeta}}_{\varphi i1} - \ddot{\boldsymbol{\varphi}}_r\right) \tag{42}$$

To handle uncertainties, the reaching control law $\boldsymbol{\tau}_{is}$ is synthesized as:

$$\boldsymbol{\tau}_{\varphi is} = -\boldsymbol{B}^{-1}_{i1}\left(\boldsymbol{\zeta}_{\varphi i2} + \hat{\boldsymbol{D}}_{\varphi i}\right) \tag{43}$$

where the vector $\boldsymbol{\zeta}_{i2} = [\zeta^1_{\varphi i2}, \zeta^2_{\varphi i2}, \zeta^3_{\varphi i2}]^{\mathrm{T}}$ is defined by the following piecewise function:

$$\zeta^p_{\varphi i2} = \begin{cases} \frac{\eta^p_{\varphi i2}(1+(z^p_{\varphi i})^2)\arctan(z^p_{\varphi i})}{T_{z_{\varphi i2}} - t + \delta^p_{\varphi i2}} & 0 \le t < T_{z_{\varphi i2}} \\ \eta^p_{\varphi i2}\left[\exp\left(\frac{\sqrt{\sigma^p_{\varphi i2}}}{\delta^p_{\varphi i2}} - \frac{\sigma^p_{\varphi i2}}{t - T_{z_{\varphi i2}} + \sqrt{\sigma^p_{\varphi i2}}\delta^p_{\varphi i2}}\right) + \frac{1}{\delta^p_{\varphi i2}} - 1\right] s_i & t \ge T_{z_{\varphi i2}} \end{cases} \tag{44}$$

in which $\eta^p_{\varphi i2}, \delta^p_{\varphi i2}, \sigma^p_{\varphi i2}$ are positive constants, and $T_{z_{\varphi i2}}$ specifies the duration of the sliding phase.

Theorem 2. *Consider the attitude tracking error system governed by (7). By applying the prescribed-time control law $\boldsymbol{\tau}_{\varphi i}$ defined as:*

$$\boldsymbol{\tau}_{\varphi i} = -\boldsymbol{B}^{-1}_{i1}\left(\dot{\boldsymbol{\zeta}}_{\varphi i1} - \ddot{\boldsymbol{\varphi}}_r + \boldsymbol{\zeta}_{\varphi i2} + \hat{\boldsymbol{D}}_{\varphi i}\right) \tag{45}$$

global tracking is achieved despite non-vanishing disturbances. Specifically, the tracking errors are guaranteed to converge to an infinitesimal neighborhood of the origin within the pre-assigned time case and remain within a compact residual set thereafter.

Proof of Theorem 2. To verify the stability of the entire scheme, we propose the following Lyapunov candidate: $L_{\varphi i1} = \frac{1}{2}\boldsymbol{z}^T_{\varphi i}\boldsymbol{z}_{\varphi i} + \frac{1}{2}\boldsymbol{z}^T_{\varphi i1}\boldsymbol{z}_{i1} + \frac{1}{2}\boldsymbol{z}^T_{\varphi i0}\boldsymbol{z}_{\varphi i0}$. Taking the time derivative of $L_{\varphi i1}$ leads to:

$$\begin{aligned} \dot{L}_{\varphi i1} &= \boldsymbol{z}^{\mathrm{T}}_{\varphi i}\dot{\boldsymbol{z}}_{\varphi i} - \boldsymbol{\zeta}_{\varphi i1}\boldsymbol{z}_{i1} - \boldsymbol{\zeta}_{\varphi i0}\boldsymbol{z}_{i0} \\ &= \boldsymbol{z}^{\mathrm{T}}_{\varphi i}\left(\boldsymbol{B}_{i1}\boldsymbol{\delta}_{i0} + \boldsymbol{D}_{\varphi i} - \ddot{\boldsymbol{\varphi}}_r + \dot{\boldsymbol{\zeta}}_{\varphi i1}\right) - \boldsymbol{\zeta}_{\varphi i1}\boldsymbol{z}_{i1} - \boldsymbol{\zeta}_{\varphi i0}\boldsymbol{z}_{i0} \end{aligned} \tag{46}$$

By substituting the control law and observer relations into the above, we obtain:

$$\begin{aligned} \dot{L}_{\varphi i1} &= \boldsymbol{z}^{\mathrm{T}}_{\varphi i}\left(-\boldsymbol{\zeta}_{\varphi 2i} - \hat{\boldsymbol{D}}_{\varphi i} + \boldsymbol{D}_{\varphi i}\right) - \boldsymbol{\zeta}_{\varphi i1}\boldsymbol{z}_{\varphi i1} - \boldsymbol{\zeta}_{\varphi i0}\boldsymbol{z}_{\varphi i0} \\ &= \boldsymbol{z}^{\mathrm{T}}_{\varphi i}\left(-\boldsymbol{\zeta}_{\varphi i2} + \tilde{\boldsymbol{D}}_{\varphi i}\right) - \boldsymbol{\zeta}_{\varphi i1}\boldsymbol{z}_{\varphi i1} - \boldsymbol{\zeta}_{\varphi i0}\boldsymbol{z}_{\varphi i0} \\ &\le -\boldsymbol{z}^{\mathrm{T}}_{\varphi i}\boldsymbol{\zeta}_{\varphi i2} + \Pi_{\varphi i} \end{aligned} \tag{47}$$

For the reaching phase $t \in [0, T_{z_{\varphi i2}})$, the following inequality holds:

$$\begin{aligned} \dot{L}_{\varphi i1} &\le -\sum_{p=1}^{3} z^p_{\varphi i}\zeta^p_{\varphi i2} + \Pi_{\varphi i} \\ &\le -\sum_{p=1}^{3} \frac{\eta^p_{\varphi i2}|z^p_{\varphi i}|(1+|(z^p_{\varphi i})^2|)\arctan(|z^p_{\varphi i}|)}{T_{z_{\varphi i2}} - t + \delta^p_{\varphi i2}} + \Pi_{\varphi i} \end{aligned} \tag{48}$$

Invoking $(1+\omega^2)\arctan(\omega) \ge \omega$, the Lyapunov derivative is bounded by:

$$\begin{aligned} \dot{L}_{\varphi i1} &\le -\sum_{p=1}^{3} \frac{\eta^p_{\varphi i2}|z^p_{\varphi i}|(1+|(z^p_{\varphi i})^2|)\arctan(|z^p_{\varphi i}|)}{T_{z_{\varphi i2}} - t + \delta^p_{\varphi i2}} + \Pi_{\varphi i} \\ &\le -\frac{\min\{\eta^1_{\varphi i2}, \eta^2_{\varphi i2}, \eta^3_{\varphi i2}\}}{T_{z_{\varphi i2}} - t + \delta'_{\varphi i2}}\left[\sum_{p=1}^{3}|z^p_{\varphi i}|(1+|(z^p_{\varphi i})^2|)\arctan(|z^p_{\varphi i}|)\right] + \Pi_{\varphi i} \\ &\le -\frac{\min\{\eta^1_{\varphi i2}, \eta^2_{\varphi i2}, \eta^3_{\varphi i2}\}}{T_{z_{\varphi i2}} - t + \delta'_{\varphi i2}}\sum_{p=1}^{3}(z^p_{\varphi i})^2 + \Pi_{\varphi i} \end{aligned} \tag{49}$$

where $\delta_{\varphi 2i}$ denotes the maximum of the time constants, $\delta'_{\varphi i2} = \max\{\delta^1_{\varphi i2}, \delta^2_{\varphi i2}, \delta^3_{\varphi i2}\}$. Let us redefine the Lyapunov components as $V_{\varphi i} = V_{\varphi i1} + V_{\varphi i2} = L_{\varphi i1}$, $V_{\varphi i1} = \sum_{p=1}^{3} \frac{1}{2}(s^p_{\varphi i})^2$, and $V_{\varphi i2} = \sum_{p=1}^{3} \frac{1}{2}(z^p_{\varphi i1})^2 + \frac{1}{2}(s^p_{\varphi i2})^2$. Then, we arrive at the following constraint:

$$\dot{V}_{\varphi i} \leq -\frac{2\min\{\eta^1_{\varphi i2}, \eta^2_{\varphi i2}, \eta^3_{\varphi i2}\}}{T_{z_{\varphi i2}} - t + \delta'_{\varphi i2}} V_{\varphi i1} + \Pi_{\varphi i} \tag{50}$$

It can thus be concluded that $V_{\varphi i}$ remains bounded.
Consequently, we have:

$$\dot{V}_{\varphi i} \leq -\frac{2\min\{\eta^1_{\varphi i2}, \eta^2_{\varphi i2}, \eta^3_{\varphi i2}\}}{T_{z_{\varphi i2}} - t + \delta'_{\varphi i2}} V_{\varphi 1} + \frac{2\min\{\eta^1_{\varphi i2}, \eta^2_{\varphi i2}, \eta^3_{\varphi i2}\}}{T_{z_{\varphi i2}} - t + \delta'_{\varphi i2}} V_{\varphi i2} + \Pi_{\varphi i} \tag{51}$$

By invoking the results from [39] and applying Gronwall's inequality, one has:

$$\begin{aligned} V_{\varphi i}(t) \leq\ & e^{-2\int_0^t \frac{\min\{\eta^1_{\varphi i2}, \eta^2_{\varphi i2}, \eta^3_{\varphi i2}\}}{T_{z_{\varphi i2}} - s + \delta'_{\varphi i2}} ds} V_{\varphi i}(0) + e^{-2\int_0^t \frac{\min\{\eta^1_{\varphi i2}, \eta^2_{\varphi i2}, \eta^3_{\varphi i2}\}}{T_{z_{\varphi i2}} - s + \delta'_{\varphi i2}} ds} \\ & \times \int_0^t \left(\frac{2\min\{\eta^1_{\varphi i2}, \eta^2_{\varphi i2}, \eta^3_{\varphi i2}\}}{T_{z_{\varphi i2}} - \varpi + \delta'_{\varphi i2}} V_{\varphi i2} + \Pi_{\varphi i} \right) e^{2\int_0^{\varpi} \frac{\min\{\eta^1_{\varphi i2}, \eta^2_{\varphi i2}, \eta^3_{\varphi i2}\}}{T_{z_{\varphi i2}} - s + \delta'_{\varphi i2}} ds} d\varpi \end{aligned} \tag{52}$$

As the time variable t approaches the pre-assigned threshold $T_{z_{\varphi i2}}$, it can be verified that $\lim_{t \to T_{z_{\varphi i2}}} V_{\varphi i}(t) \leq V_{\varphi i}(0) \exp\left(-2\int_0^t \frac{\min\{\eta^1_{\varphi i2}, \eta^2_{\varphi i2}, \eta^3_{\varphi i2}\}}{T_{z_{\varphi i2}} - s + \delta'_{\varphi i2}} \right) ds$ vanishes. Consequently, the Lyapunov function is bounded by:

$$V_{\varphi i} \leq e^{-2\int_0^t \frac{\min\{\eta^1_{\varphi i2}, \eta^2_{\varphi i2}, \eta^3_{\varphi i2}\}}{T_{z_{\varphi i2}} - s + \delta'_{\varphi i2}} ds} \int_0^t \left(\frac{2\min\{\eta^1_{\varphi i2}, \eta^2_{\varphi i2}, \eta^3_{\varphi i2}\}}{T_{z_{\varphi i2}} - \varpi + \delta'_{\varphi i2}} V_{\varphi i2} + \Pi_{\varphi i} \right) e^{2\int_0^{\varpi} \frac{\min\{\eta^1_{\varphi i2}, \eta^2_{\varphi i2}, \eta^3_{\varphi i2}\}}{T_{z_{\varphi i2}} - s + \delta'_{\varphi i2}} ds} d\varpi \tag{53}$$

Furthermore, by employing L'Hospital's rule, it is demonstrated as:

$$\begin{aligned} \lim_{t \to T^-_{z_{\varphi i2}}} V_{\varphi i} \leq & \lim_{t \to T^-_{z_{\varphi i2}}} \frac{\int_0^t \left(\frac{2\min\{\eta^1_{\varphi i2}, \eta^2_{\varphi i2}, \eta^3_{\varphi i2}\}}{T_{z_{\varphi i2}} - \varpi + \delta'_{\varphi i2}} V_{\varphi i2} + \Pi_{\varphi i} \right) e^{2\int_0^t \frac{\min\{\eta^1_{\varphi i2}, \eta^2_{\varphi i2}, \eta^3_{\varphi i2}\}}{T_{z_{\varphi i2}} - \varpi + \delta'_{\varphi i2}} ds} d\varpi}{e^{2\int_0^{'} \frac{\min\{\eta^1_{\varphi i2}, \eta^2_{\varphi i2}, \eta^3_{\varphi i2}\}}{T_{z_{\varphi i2}} + \delta'_{\varphi i2} - s} ds}} \\ \leq & \lim_{t \to T^-_{z_{\varphi i2}}} \frac{\left(\frac{2\min\{\eta^1_{\varphi i2}, \eta^2_{\varphi i2}, \eta^3_{\varphi i2}\}}{T_{z_{\varphi i2}} - t + \delta'_{\varphi i2}} V_{\varphi i2} + \Pi_{\varphi i} \right) e^{2\int_0^t \frac{\min\{\eta^1_{\varphi i2}, \eta^2_{\varphi i2}, \eta^3_{\varphi i2}\}}{T_{z_{\varphi i2}} - s + \delta'_{\varphi i2}} ds}}{\frac{2\min\{\eta^1_{\varphi i2}, \eta^2_{\varphi i2}, \eta^3_{\varphi i2}\}}{T_{z_{\varphi i2}} + \delta'_{\varphi i2} - t} e^{2\int_0^t \frac{\min\{\eta^1_{\varphi i2}, \eta^2_{\varphi i2}, \eta^3_{\varphi i2}\}}{T_{z_{\varphi i2}} - s + \delta'_{\varphi i2}} ds}} \\ \leq & \lim_{t \to T^-_{z_{\varphi i2}}} V_{\varphi i2} + \frac{(T_{z_{\varphi i2}} + \delta'_{\varphi i2} - t)\Pi_{\varphi i}}{2\min\{\eta^1_{\varphi i2}, \eta^2_{\varphi i2}, \eta^3_{\varphi i2}\}} \end{aligned} \tag{54}$$

From the above derivation, it is evident that:

$$\lim_{t \to T^-_{z_{\varphi i2}}} \frac{(T_{z_{\varphi i2}} + \delta'_{\varphi i2} - t)\Pi_{\varphi i}}{2\min\{\eta^1_{\varphi i2}, \eta^2_{\varphi i2}, \eta^3_{\varphi i2}\}} = a_{\varphi i1} \tag{55}$$

Ultimately, through the selection of appropriate control parameters, it can be ascertained that $\lim_{t \to T_{z_{\varphi i2}}} V_{\varphi i1} \leq a_{\varphi i1}$. This confirms that the state tracking error enters the bound $a_{\varphi i1}$ within the prescribed time horizon $T_{z_{\varphi i2}}$.

For $t \in [T_{z_{\varphi i2}}, +\infty)$, the evolution of the Lyapunov candidate is expressed as:

$$\begin{aligned}\dot{V}_{\varphi i}(t) &= \dot{V}_{\varphi i1}(t) + \dot{V}_{\varphi i2} \le -\boldsymbol{z}_{\varphi i}^{\mathrm{T}}\boldsymbol{\zeta}_{\varphi i2} + \Pi_{\varphi i} \\ &\le -\sum_{p=1}^{3}\eta_{\varphi i2}^{p}\left[\exp\left(\frac{\sqrt{\sigma_{\varphi i2}^{p}}}{\delta_{\varphi i2}^{p}} - \frac{\sigma_{\varphi i2}^{p}}{t - T_{z_{\varphi i2}} + \sqrt{\sigma_{\varphi i2}^{p}}\delta_{\varphi i2}^{p}}\right) + \frac{1}{\delta_{\varphi i2}^{p}} - 1\right](z_{\varphi i}^{p})^2 + \Pi_{\varphi i} \\ &\le -2\eta'_{\varphi i2}\left[\exp\left(\frac{\sqrt{\sigma'_{\varphi i2}}}{\delta'_{\varphi i2}} - \frac{\sigma'_{\varphi i2}}{t - T_{z_{\varphi i2}} + \sqrt{\sigma'_{\varphi i2}}\delta'_{\varphi i2}}\right) + \frac{1}{\delta'_{\varphi i2}} - 1\right]V_{\varphi i1} \\ &\quad + 2\eta'_{\varphi i2}\left[\exp\left(\frac{\sqrt{\sigma'_{\varphi i2}}}{\delta'_{\varphi i2}} - \frac{\sigma'_{\varphi i2}}{t - T_{z_{\varphi i2}} + \sqrt{\sigma'_{\varphi i2}}\delta'_{\varphi i2}}\right) + \frac{1}{\delta'_{\varphi i2}} - 1\right]V_{\varphi i2} + \Pi_{\Pi i}\end{aligned} \tag{56}$$

where we denote $\sigma'_{\varphi i2} = \min\{\sigma_{\varphi i2}^1, \sigma_{\varphi i2}^2, \sigma_{\varphi i2}^3\}^T$ and $\eta'_{\varphi i2} = \min\{\eta_{\varphi i2}^1, \eta_{\varphi i2}^2, \eta_{\varphi i2}^3\}^T$. In light of Gronwall's lemma and the methodology in [39], the solution satisfies:

$$\begin{aligned}V_{\varphi i}(t) \le\ & e^{-2\eta'_{\varphi i2}\int_{T_{z_{\varphi i2}}}^{t}\left[\exp\left(\frac{\sqrt{\sigma'_{\varphi i2}}}{\delta'_{\varphi i2}} - \frac{\sigma'_{\varphi i2}}{s - T_{z_{\varphi i2}} + \sqrt{\sigma'_{\varphi i2}}\delta'_{\varphi i2}}\right) + \frac{1}{\delta'_{\varphi i2}} - 1\right]ds} \\ & \times \int_{T_{z_{\varphi i2}}}^{t}\left(2\eta'_{\varphi i2}\left[\exp\left(\frac{\sqrt{\sigma'_{\varphi i2}}}{\delta'_{\varphi i2}} - \frac{\sigma'_{\varphi i2}}{\varpi - T_{z_{\varphi i2}} + \sqrt{\sigma'_{\varphi i2}}\delta'_{\varphi i2}}\right) + \frac{1}{\delta'_{\varphi i2}} - 1\right]V_{\varphi i2} + \Pi_{\varphi i}\right)d\varpi \\ & \times e^{2\eta'_{\varphi i2}\int_{T_{z_{\varphi i2}}}^{\varpi}\left[\exp\left(\frac{\sqrt{\sigma'_{\varphi i2}}}{\delta'_{\varphi i2}} - \frac{\sigma'_{\varphi i2}}{s - T_{z_{\varphi i2}} + \sqrt{\sigma'_{\varphi i2}}\delta'_{\varphi i2}}\right) + \frac{1}{\delta'_{\varphi i2}} - 1\right]ds}d\varpi \\ & + e^{-2\eta'_{\varphi i2}\int_{T_{z_{\varphi i2}}}^{t}\left[\exp\left(\frac{\sqrt{\sigma'_{\varphi i2}}}{\delta'_{\varphi i2}} - \frac{\sigma'_{\varphi i2}}{s - T_{z_{\varphi i2}} + \sqrt{\sigma'_{\varphi i2}}\delta'_{\varphi i2}}\right) + \frac{1}{\delta'_{\varphi i2}} - 1\right]ds}V_{\varphi i}(T_{z_{\varphi i2}})\end{aligned} \tag{57}$$

As time tends toward infinity ($t \to \infty$), the transient term associated with $V_{\varphi i}(T_{z_{\varphi i2}})$ decays to zero. Thus, the steady-state bound is obtained as:

$$\begin{aligned}\lim_{t\to\infty} V_{\varphi i}(t) \le\ & \frac{1}{\lim_{t\to\infty} e^{2\eta'_{\varphi i2}\int_{T_{z_{\varphi i2}}}^{t}\left[\exp\left(\frac{\sqrt{\sigma'_{\varphi i2}}}{\delta'_{\varphi i2}} - \frac{\sigma'_{\varphi i2}}{s - T_{z_{\varphi i2}} + \sqrt{\sigma'_{\varphi i2}}\delta'_{\varphi i2}}\right) + \frac{1}{\delta'_{\varphi i2}} - 1\right]ds}} \times \\ & \lim_{t\to\infty}\int_{T_{z_{\varphi i2}}}^{t}\left(2\eta'_{\varphi i2}\left[\exp\left(\frac{\sqrt{\sigma'_{\varphi i2}}}{\delta'_{\varphi i2}} - \frac{\sigma'_{\varphi i2}}{\varpi - T_{z_{\varphi i2}} + \sqrt{\sigma'_{\varphi i2}}\delta'_{\varphi i2}}\right) + \frac{1}{\delta'_{\varphi i2}} - 1\right]V_{\varphi i2} + \Pi_{\varphi i}\right) \times \\ & e^{2\eta'_{\varphi i2}\int_{T_{z_{\varphi i2}}}^{\varpi}\left[\exp\left(\frac{\sqrt{\sigma'_{\varphi i2}}}{\delta'_{\varphi i2}} - \frac{\sigma'_{\varphi i2}}{s - T_{z_{\varphi i2}} + \sqrt{\sigma'_{\varphi i2}}\delta'_{\varphi i2}}\right) + \frac{1}{\delta'_{\varphi i2}} - 1\right]ds}d\varpi \\ & \le V_{\varphi i2} + \frac{\Pi_{\varphi i}}{2\eta'_{\varphi i2}\left[\exp\left(\frac{\sqrt{\sigma'_{\varphi i2}}}{\sigma'_{\varphi i2}}\right) + \frac{1}{\sigma'_{\varphi i2}} - 1\right]}\end{aligned} \tag{58}$$

In a similar manner, by tuning the design parameters, we can show that:

$$\lim_{t\to\infty} V_{\varphi i1}(t) \le \frac{\delta'_{\varphi i2}\Pi_{\varphi i}}{2\eta'_{\varphi i2}\left[\delta'_{\varphi i2}\exp\left(\frac{\sqrt{\sigma'_{\varphi i2}}}{\delta'_{\varphi i2}}\right) + 1 - \delta'_{\varphi i2}\right]} = a_{\varphi i2} \tag{59}$$

In conclusion, the Lyapunov function $V_{\varphi i}$ is confirmed to be bounded, ensuring that the system trajectories converge to a predefined residual set within the specified time $T_{z_{\varphi i2}}$ and remain stable thereafter. □

Theorem 3. *Upon the sliding manifold reaching the region $a_{\varphi i2}$, the error states $\boldsymbol{e}_{\varphi i1}$ and $\boldsymbol{e}_{\varphi i2}$ are guaranteed to settle within a small neighborhood of the origin within a finite time $T_{z_{\varphi i1}}$, thereby fulfilling the requirements for practical prescribed-time stability.*

Proof of Theorem 3. Through the meticulous selection of design parameters, the convergence region can be tuned to be infinitesimally small. Depending on the specific value of $a_{\varphi i2}$, the stability analysis is bifurcated into the following two cases.

Case 1: We first consider the case where the sliding manifold has reached the vicinity of the origin. From the relation in (42) and (43), it follows that $\dot{\boldsymbol{e}}_{\varphi i1} = -\boldsymbol{\zeta}_{\varphi i1}$. To evaluate the convergence, a Lyapunov candidate is defined as $W_\varphi = \frac{1}{2}\boldsymbol{e}_{\varphi i1}^T \boldsymbol{e}_{\varphi i1}$.

During the reaching phase $t \in [0, T_{z_{\varphi i1}})$, the temporal derivative of the Lyapunov function is given by:

$$\begin{aligned} \dot{W}_{\varphi i} &= \boldsymbol{e}_{\varphi i1}^{\mathrm{T}} \dot{\boldsymbol{e}}_{\varphi i1} = -\boldsymbol{e}_{\varphi i1}^{\mathrm{T}} \zeta_{\varphi i1} = -\sum_{p=1}^{3} \frac{\eta_{\varphi i1}^{p} |e_{\varphi i1}^{p}| (1 + (e_{\varphi i1}^{p})^2) \arctan(|e_{\varphi i1}^{p}|)}{T_{z_{\varphi i1}} - t + \delta_{\varphi i1}^{p}} \\ &\leq -\frac{\min\{\eta_{\varphi i1}^{1}, \eta_{\varphi i1}^{2}, \eta_{\varphi i1}^{3}\}}{T_{z_{\varphi i1}} - t + \delta'_{\varphi i1}} \sum_{p=1}^{3} e_{\varphi i1}^{2} = -\frac{2\eta'_{\varphi i1}}{T_{z_{\varphi i1}} - t + \delta'_{\varphi i1}} W_{\varphi i} \end{aligned} \tag{60}$$

where $\eta'_{\varphi i1} = \min\{\eta_{\varphi i1}^{1}, \eta_{\varphi i1}^{2}, \eta_{\varphi i1}^{3}\}$ and $\delta'_{\varphi i1} = \max\{\delta_{\varphi i1}^{1}, \delta_{\varphi i1}^{2}, \delta_{\varphi i1}^{3}\}$ are consolidated parameters. By integrating this differential inequality via Gronwall's Lemma, it is derived:

$$\begin{aligned} \dot{W}_{\varphi i} &\leq \dot{W}_{\varphi i}(0) \exp\left(\int_0^{T_{z_{\varphi i1}}} -\frac{\eta'_{\varphi i1}}{T_{z_{\varphi i1}} - s + \delta'_{\varphi i1}} ds \right) \\ &\leq \dot{W}_{\varphi i}(0) \exp\left[\int_0^{T_{z_{\varphi i1}}} \frac{2\eta'_{\varphi i1}}{T_{z_{\varphi i1}} - s + \delta'_{\varphi i1}} d(T_{z_{\varphi i1}} - s + \delta'_{\varphi i1}) \right] \\ &\leq \dot{W}_{\varphi i}(0) \left(1 - \frac{t}{T_{z_{\varphi i1}} + \delta'_{\varphi i1}} \right)^{2\eta'_{\varphi i1}} = a_{\varphi i3} \end{aligned} \tag{61}$$

Consequently, as $t \to T_{z_{\varphi i1}}$, the tracking error converges within the residual set $a_{\varphi i3}$. For $t \in [T_{z_{\varphi i1}}, \infty)$, the dynamics are expressed as:

$$\begin{aligned} \dot{W}_{\varphi i} &= \boldsymbol{e}_{\varphi i1}^{\mathrm{T}} \dot{\boldsymbol{e}}_{\varphi i1} = -\boldsymbol{e}_{\varphi i1}^{\mathrm{T}} \boldsymbol{\zeta}_{\varphi i1} \\ &\leq -2 \left[\exp\left(\frac{\sqrt{\sigma'_{\varphi i1}}}{\delta'_{\varphi i1}} - \frac{\sigma'_{\varphi i1}}{t - T_{z_{\varphi i1}} + \sqrt{\sigma'_{\varphi i1}} \delta'_{\varphi i1}} \right) + \frac{\eta'_{\varphi i1}}{\delta'_{\varphi i1}} - 1 \right] W_{\varphi i} \end{aligned} \tag{62}$$

where $\sigma'_{\varphi i1} = \min\{\sigma_{\varphi i1}^{1}, \sigma_{\varphi i1}^{2}, \sigma_{\varphi i1}^{3}\}$. Drawing upon Gronwall's inequality and the methodology in [39], it follows that:

$$\dot{W}_{\varphi i}(t) \leq \dot{W}_{\varphi}(T_{z_{\varphi i1}}) e^{\int_{T_{z_{\varphi i1}}}^{t} -2 \left[\exp\left(\frac{\sqrt{\sigma'_{\varphi i1}}}{\delta'_{\varphi i1}} - \frac{\sigma'_{\varphi i1}}{s - T_{z_{\varphi i1}} + \sqrt{\sigma'_{\varphi i1}} \delta'_{\varphi i1}} \right) + \frac{\eta'_{\varphi i1}}{\delta'_{\varphi i1}} - 1 \right] ds} \tag{63}$$

Note that the exponential term within the integral is a monotonically increasing function. Utilizing the definition of the derivative and the integral property, we have:

$$\int_{T_{z_{\varphi i1}}}^{t} -2\left[\exp\left(\frac{\sqrt{\sigma'_{\varphi i1}}}{\delta'_{\varphi i1}} - \frac{\sigma'_{\varphi i1}}{s - T_{z_{\varphi i1}} + \sqrt{\sigma'_{\varphi i1}}\delta'_{\varphi i1}}\right) + \frac{\eta'_{\varphi i1}}{\delta'_{\varphi i1}} - 1\right] ds \leq -2\frac{\eta'_{\varphi i1}}{\delta'_{\varphi i1}}(t - T_{z_{\varphi i1}}) \quad (64)$$

Thus, (71) is simplified to the following form:

$$\dot{W}_{\varphi i}(t) \leq \dot{W}_{\varphi i}\left(T_{z_{\varphi i1}}\right) e^{-2\frac{\eta'_{\varphi i1}}{\delta'_{\varphi i1}}(t - T_{z_{\varphi i1}})} \quad (65)$$

In the limit as $t \to \infty$, we obtain $\lim_{t\to\infty} \dot{W}_{\varphi i} \leq \lim_{t\to\infty} \dot{W}_{\varphi i}\left(T_{z_{\varphi i1}}\right) e^{-2\frac{\eta'_{\varphi i1}}{\delta'_{\varphi i1}}(t - T_{z_{\varphi i1}})} = a_{\varphi i4}$, Therefore, the state variable s is confirmed to settle within the bound $a_{\varphi i4}$ within the pre-assigned time $T_{z_{\varphi i2}}$.

Case 2: Consider the case where $z_{\varphi i} \neq 0$, and the convergence of the tracking error is represented by $\mathbf{\Gamma}_{\varphi i} = [\Gamma_{\varphi i1}, \Gamma_{\varphi i2}, \Gamma_{\varphi i3}]^{\mathrm{T}}$. The sliding surface relation $z_{\varphi i} = \dot{e}_{\varphi i1} + \zeta_{\varphi i1} = \mathbf{\Gamma}_{\varphi i}$ implies that the error rate is $\dot{e}^p_{\varphi i} = \mathbf{\Gamma}^p_{\varphi i} - \zeta^p_{\varphi i1}$. We proceed to analyze each error component $e^p_{\varphi i}$ individually for $p = 1, 2, 3$.

For $t \in [0, T_{z_{\varphi i1}})$, the error dynamics satisfy:

$$\begin{aligned} \dot{e}^p_{\varphi i1}(t) &= -\zeta^p_{\varphi i1} + \Gamma^p_{\varphi i} = -\frac{\eta^p_{\varphi i1}(1 + (e^p_{\varphi i1})^2)\arctan(e^p_{\varphi i1})}{T_{z_{\varphi i1}} - t + \delta^p_{\varphi i1}} + \Gamma^p_{\varphi i} \\ &\leq -\frac{\eta^p_{\varphi i1}}{T_{z_{\varphi i1}} - t + \delta^p_{\varphi i1}} e_{\varphi i1} + \Gamma^p_{\varphi i} \end{aligned} \quad (66)$$

In accordance with [39] and applying Gronwall's Lemma, we yield:

$$\begin{aligned} e^p_{\varphi i1} &\leq \exp\left(\int_0^{\mathrm{T}} -\frac{\eta^p_{\varphi i1}}{T_{z_{\varphi i1}} - t + \delta^p_{\varphi i1}} ds\right) e^p_{\varphi i1}(0) \\ &\quad + \exp\left(\int_0^{\mathrm{T}} -\frac{\eta^p_{\varphi i1}}{T_{z_{\varphi i1}} - t + \delta^p_{\varphi i1}} ds\right) \int_0^{\mathrm{T}} \Gamma^p_{\varphi i1} \exp\left(\int_0^{\varpi} \frac{\eta^p_{\varphi i1}}{T_{z_{\varphi i1}} - s + \delta^p_{\varphi i1}} ds\right) d\varpi \\ &\leq e_{\varphi i1}(0)\left(1 - \frac{t}{T_{z_{\varphi i1}} + \delta^p_{\varphi i1}}\right)^{\eta^p_{\varphi i1}} \\ &\quad + \frac{\Gamma^p_{\varphi i1}(T_{z_{\varphi i1}} + \delta^p_{\varphi i1})\eta^p_{\varphi i1}}{1 - \eta^p_{\varphi i1}}\left[\left(T_{z_{\varphi i1}} - t + \delta^p_{\varphi i1}\right)^{1-\eta^p_{\varphi i1}} - \left(T_{z_{\varphi i1}} + \delta^p_{\varphi i1}\right)^{1-\eta^p_{\varphi i1}}\right] \end{aligned} \quad (67)$$

As time approaches the threshold $T_{z_{\varphi i1}}$, the limit of the tracking error is given by:

$$\begin{aligned} \lim_{t\to T_{z_{\varphi i1}}} e^p_{\varphi i1}(t) &\leq \lim_{t\to T_i} e^p_{\varphi i1}(0)\left(\frac{\delta^p_{\varphi i1}}{T_{z_{\varphi i1}} + \delta^p_{\varphi i1}}\right)^{\eta^p_{\varphi i1}} \\ &\quad + \frac{\Gamma^p_{\varphi i}(T_{z_{\varphi i1}} + \delta^p_{\varphi i1})^{\eta^p_{\varphi i1}}}{1 - \eta^p_{\varphi i1}}\left[\left(\delta^p_{\varphi i1}\right)^{1-\eta^p_{\varphi i1}} - \left(T_{z_{\varphi i1}} + \delta^p_{\varphi i1}\right)^{1-\eta^p_{\varphi i1}}\right] = a_{\varphi i5}, \end{aligned} \quad (68)$$

Through the proper selection of parameters, the convergence of the tracking error to the set $a_{\varphi i5}$ is ensured.

For $t \in [T_{z_{\varphi i1}}, \infty)$, the system satisfies:

$$\dot{e}_{\varphi i1} = -\left[\exp\left(\frac{\sqrt{\sigma^p_{\varphi i1}}}{\delta^p_{\varphi i1}} - \frac{\sigma^p_{\varphi i1}}{t - T_{z_{\varphi i1}} + \sqrt{\sigma^p_{\varphi i1}}\delta^p_{\varphi i1}}\right) + \frac{\eta^p_{\varphi i1}}{\delta^p_{\varphi i1}} - 1\right] e^p_{\varphi i1} + \Gamma^p_{\varphi i} \tag{69}$$

By invoking Gronwall's Lemma once more, we have:

$$\begin{aligned} e^p_{\varphi i1}(t) \le\ & e^p_{\varphi i1}(T_{z_{\varphi i1}}) e^{\int_{T_{z_{\varphi i1}}}^{t}\left[\exp\left(\frac{\sqrt{\sigma^p_{\varphi i1}}}{\delta^p_{\varphi i1}} - \frac{\sigma^p_{\varphi i1}}{s - T_{z_{\varphi i1}} + \sqrt{\sigma^p_{\varphi i1}}\delta^p_{\varphi i1}}\right) + \frac{\eta^p_{\varphi i1}}{\delta^p_{\varphi i1}} - 1\right] ds} \\ & + e^{\int_{T_{z_{\varphi i1}}}^{t}\left[\exp\left(\frac{\sqrt{\sigma^p_{\varphi i1}}}{\delta^p_{\varphi i1}} - \frac{\sigma^p_{\varphi i1}}{s - T_{z_{\varphi i1}} + \sqrt{\sigma^p_{\varphi i1}}\delta^p_{\varphi i1}}\right) + \frac{\eta^p_{\varphi i1}}{\delta^p_{\varphi i1}} - 1\right] ds} \\ & \times \int_{T_{z_{\varphi i1}}}^{t} \Gamma^p_{\varphi i} e^{\int_{T_{z_{\varphi i1}}}^{\varpi}\left[\exp\left(\frac{\sqrt{\sigma^p_{\varphi i1}}}{\delta^p_{\varphi i1}} - \frac{\sigma^p_{\varphi i1}}{s - T_{z_{\varphi i1}} + \sqrt{\sigma^p_{\varphi i1}}\delta^p_{\varphi i1}}\right) + \frac{\eta^p_{\varphi i1}}{\delta^p_{\varphi i1}} - 1\right] ds} d\varpi \\ \le\ & e^p_{\varphi i1}(T_{z_{\varphi i1}}) e^{-(t - T_{z_{\varphi i1}})\frac{\eta^p_{\varphi i1}}{\delta^p_{\varphi i1}}} + e^{\int_{T_{z_{\varphi i1}}}^{t}\left[\exp\left(\frac{\sqrt{\sigma^p_{\varphi i1}}}{\delta^p_{\varphi i1}} - \frac{\sigma^p_{\varphi i1}}{s - T_{z_{\varphi i1}} + \sqrt{\sigma^p_{\varphi i1}}\delta^p_{\varphi i1}}\right) + \frac{\eta^p_{\varphi i1}}{\delta^p_{\varphi i1}} - 1\right] ds} \\ & \times \int_{T_{z_{\varphi i1}}}^{t} \Gamma^p_{\varphi i} e^{\int_{T_{z_{\varphi i1}}}^{\varpi}\left[\exp\left(\frac{\sqrt{\sigma^p_{\varphi i1}}}{\delta^p_{\varphi i1}} - \frac{\sigma^p_{\varphi i1}}{s - T_{z_{\varphi i1}} + \sqrt{\sigma^p_{\varphi i1}}\delta^p_{\varphi i1}}\right) + \frac{\eta^p_{\varphi i1}}{\delta^p_{\varphi i1}} - 1\right] ds} d\varpi \end{aligned} \tag{70}$$

In the limit as $t \to \infty$, it is found that:

$$\begin{aligned} \lim_{t\to\infty} e^p_{\varphi i1} &\le \lim_{t\to\infty} \frac{\int_{T_{z_{\varphi i1}}}^{t} \Gamma^p_{\varphi i} \exp\left[\int_{T_{z_{\varphi i1}}}^{\varpi}\left[\exp\left(\frac{\sqrt{\sigma^p_{\varphi i1}}}{\delta^p_{\varphi i1}} - \frac{\sigma^p_{\varphi i1}}{s - T_{z_{\varphi i1}} + \sqrt{\sigma^p_{\varphi i1}}\delta^p_{\varphi i1}}\right) + \frac{\eta^p_{\varphi i1}}{\delta^p_{\varphi i1}} - 1\right] ds\right] d\varpi}{e^{\int_{T_{z_{\varphi i1}}}^{t}\left[\exp\left(\frac{\sqrt{\sigma^p_{\varphi i1}}}{\delta^p_{\varphi i1}} - \frac{\sigma^p_{\varphi i1}}{s - T_{z_{\varphi i1}} + \sqrt{\sigma^p_{\varphi i1}}\delta^p_{\varphi i1}}\right) + \frac{\eta^p_{\varphi i1}}{\delta^p_{\varphi i1}} - 1\right] ds}} \\ &\le \lim_{t\to\infty} \frac{\Gamma^p_{\varphi i}(t - T_{z_{\varphi i1}})}{\exp\left(\frac{\sqrt{\sigma^p_{\varphi i1}}}{\delta^p_{\varphi i1}}\right) + \frac{\eta^p_{\varphi i1}}{\delta^p_{\varphi i1}} - 1} = a_{\varphi i6} \end{aligned} \tag{71}$$

This demonstrates that the tracking error remains confined within a minute residual domain. In conclusion, based on Definition 1, we have verified that the proposed control framework achieves practical prescribed-time stability for the attitude system. This concludes the proof. □

3.2. Prescribed-Time Sliding Mode Controller for Translational Subsystem

The velocity tracking deviation is characterized by $e_{vi} = V_i - V_0$, where V_0 represents the reference speed commanded by the virtual leader. By differentiating e_{vi} with respect to time, the first-order error dynamics are formulated as:

$$\dot{e}_{vi} = f_{vi} + g_{vi} F_{Txi0} + D_{Vi} - \dot{V}_d \tag{72}$$

The primary control aim consists of synthesizing the thrust command F_{Txi0} such that the speed error e_{vi} is driven into a minute neighborhood of the origin within a pre-stipulated time T_{vi}, even under the influence of the unknown and non-vanishing perturbation D_{Vi}.

3.2.1. Prescribed-Time Sliding Mode Observer

In view of the fact that flight integrity is often compromised by unknown aerodynamic disturbances and potential thrust inefficiencies D_{Vi}, we develop a reduced-order scalar observer based on prescribed-time sliding mode theory to achieve high-precision estimation.

To this end, define an auxiliary variable $\vartheta_{vi} = -l_{v1}\int_0^{\mathrm{T}}(f_{vi} + g_{vi}F_{Txi0} + l_{v2}\vartheta_{vi})d\nu + l_{v1}V_i$, where l_{v1} and l_{v2} denote positive design constants for the observer. The temporal evolution of this state is governed by $\dot{\vartheta}_{vi} = -l_{v1}l_{v2}\vartheta_{vi} + l_{v1}D_{Vi}$, which effectively functions as a first-order filter for the lumped disturbance term. By letting $z_{vi0} = \vartheta_{vi} - \hat{\vartheta}_{vi}$ represent the estimation discrepancy, a scalar integral-type sliding manifold z_{vi1} is constructed $z_{vi1} = \dot{z}_{vi0} + \int_0^{\mathrm{T}}\zeta_{vi0}d\nu$.

Theorem 4. *Under the framework of the translational subsystem's first-order dynamics for a fixed-wing UAV, consider the following sliding mode disturbance observer:*

$$\begin{cases} \dot{\hat{\vartheta}}_{vi} = \zeta_{vi1} + \zeta_{vi0} + \int_0^{\mathrm{T}}\zeta_{vi0}d\nu \\ \hat{D}_{Vi} = l_{vi2}\hat{\vartheta}_{vi} + l_{vi1}^{-1}\dot{\hat{\vartheta}}_{vi} \end{cases} \tag{73}$$

In this structure, $\hat{D}_{Vi}$ signifies the estimated value of the unknown disturbance D_{Vi}, while ζ_{vi0} and ζ_{vi1} are defined as scalar prescribed-time reference convergence differential functions following:

$$\zeta_{vi0} = \begin{cases} \frac{k_{vi1}(1+z_{v0i}^2)\arctan(z_{v0i})}{T_{z_{vi0}}-t+k_{vi3}} & 0 \le t < T_{z_{vi0}} \\ \left[\exp\left(\frac{\sqrt{k_{vi2}}}{k_{vi3}} - \frac{k_{vi2}}{t-T_{z_{vi0}}+\sqrt{k_{vi2}}k_{vi3}}\right) + \frac{k_{vi1}}{k_{vi3}} - 1\right]z_{vi0} & t \ge T_{z_{vi0}} \end{cases} \tag{74}$$

$$\zeta_{vi1} = \begin{cases} \frac{k_{vi4}(1+z_{vi1}^2)\arctan(z_{vi1})}{T_{z_{vi1}}-t+k_{vi6}} & 0 \le t < T_{z_{vi1}} \\ \left[\exp\left(\frac{\sqrt{k_{vi4}}}{k_{vi6}} - \frac{k_{vi5}}{t-T_{z_{vi1}}+\sqrt{k_{vi2}}k_{vi6}}\right) + \frac{k_{vi4}}{k_{vi6}} - 1\right]z_{vi1} & t \ge T_{z_{vi1}} \end{cases} \tag{75}$$

where $k_{vi1}, k_{vi2}, k_{vi3}, k_{vi4}, k_{vi5}, k_{vi6}$ are positive constants, with $k_{vi1} > k_{vi3}$, $k_{vi4} > k_{vi6}$, $T_{z_{vi0}}$ and $T_{z_{vi1}}$ are prescribed time; the convergence of the estimation error $\tilde{D}_{Vi} = D_{Vi} - \hat{D}_{Vi}$ to zero is guaranteed within time horizon $T_{z_{vi0}} + T_{z_{vi1}}$.

Proof of Theorem 4. Utilizing the observer dynamics, the derivative of the sliding variable can be described by $\dot{z}_{vi1} = -\zeta_{vi1}$. To evaluate the stability of this sliding manifold, we select the following Lyapunov candidate $L_{z_{vi1}} = \frac{1}{2}z_{vi1}^2$. Based on the prescribed convergence time $T_{z_{vi1}}$, the analysis is partitioned into two temporal phases:

Case 1: For $t \in [0, T_{z_{vi1}})$, the time derivative of the Lyapunov function yields:

$$\dot{L}_{z_{vi1}} = z_{vi1}\dot{z}_{vi1} = -z_{vi1}\zeta_{vi1} = -\frac{k_{vi4}|z_{vi1}|(1+z_{vi1}^2)\arctan(|z_{vi1}|)}{T_{z_{vi1}}-t+k_{vi6}} \tag{76}$$

By defining the auxiliary mapping $\epsilon(z_{vi1}) = (1+z_{vi1}^2)\arctan(|z_{vi1}|)$ and invoking the properties of convex functions from Lemma 1 and Lemma 3, the derivative can be bounded as:

$$\dot{L}_{z_{vi1}} \le -\frac{k_{vi4}\sqrt{2L_{z_{vi1}}}\epsilon(\sqrt{2L_{z_{vi1}}})}{T_{z_{vi1}}-t+k_{vi6}} \tag{77}$$

We introduce the auxiliary variable $m_{vi1} = \sqrt{2L_{z_{vi1}}}$. Its dynamic evolution satisfies the following inequality $\dot{m}_{vi1} = \frac{\dot{L}_{z_{vi1}}}{\sqrt{2L_{z_{vi1}}}} \leq -\frac{k_{vi4}\epsilon(m_{vi1})}{T_{z_{vi1}}-t+k_{vi6}}$. Further, utilizing the property $\epsilon(m_{vi1}) = (1+m_{vi1}^2)\arctan(m_{vi1}) \geq m_{vi1}$, it can be obtained that:

$$\dot{m}_{vi1} \leq -\frac{k_{vi4}(1+m_{vi1}^2)\arctan(m_{vi1})}{T_{z_{vi1}}-t+k_{vi6}} \leq -\frac{k_{vi4}m_{vi1}}{T_{z_{vi1}}-t+k_{vi6}} \tag{78}$$

By integrating both sides, we obtain

$$m_{vi1}(t) \leq m_{vi1}(0)\left(\frac{T_{z_{vi1}}-t+k_{vi6}}{T_{z_{vi1}}+k_{vi6}}\right)^{k_{vi4}} \tag{79}$$

This demonstrates that, with an appropriate selection of observer parameters, m_{vi1} and $L_{z_{vi1}}$ converge to a minute neighborhood of the origin before $t = T_{z_{vi1}} + k_{vi6}$. By invoking the squeeze theorem, we confirm that the sliding variable z_{vi1} reaches equilibrium exactly at the prescribed time.

Case 2: For the steady-state phase $t \in [T_{z_{vi1}}, \infty)$, due to the introduction of the exponential decay term in the piecewise function, the system dynamics satisfy:

$$\begin{aligned}\dot{L}_{z_{vi1}} &= -\left[\exp\left(\frac{\sqrt{k_{vi5}}}{k_{vi6}} - \frac{k_{vi5}}{t-T_{z_{vi1}}+\sqrt{k_{vi5}}k_{vi6}}\right) + \frac{k_{vi4}}{k_{vi6}} - 1\right] z_{vi1}^2 \\ &\leq -2\left[\exp\left(\frac{\sqrt{k_{vi5}}}{k_{vi6}} - \frac{k_{vi5}}{t-T_{z_{vi1}}+\sqrt{k_{vi5}}k_{vi6}}\right) + \frac{k_{vi4}}{k_{vi6}} - 1\right] L_{z_{vi1}}\end{aligned} \tag{80}$$

Through the application of Gronwall's lemma, it follows that:

$$L_{z_{vi1}}(t) \leq L_{z_{vi1}}(T_{z_{vi1}})e^{\left(-2\int_{T_{z_{vi1}}}^{T}\left[\exp\left(\frac{\sqrt{k_{vi5}}}{k_{vi6}} - \frac{k_{vi5}}{s-T_{z_{vi1}}+\sqrt{k_{vi5}}k_{vi6}}\right) + \frac{k_{vi4}}{k_{vi6}} - 1\right]ds\right)} \tag{81}$$

Hence, by tuning the parameters, the observation error $L_{z_{vi1}}$ is maintained within a negligible bound after the specified time. This confirms that the sliding manifold z_{vi1} achieves prescribed-time convergence.

Once the sliding manifold is reached (i.e., $z_{vi1} \to 0$), the error dynamics simplify to $\dot{z}_{vi0} = -\zeta_{vi0}$. We define a similar Lyapunov candidate function $L_{z_{vi0}} = \frac{1}{2}z_{vi0}^2$ for the estimation discrepancy.

Case 1: For $t \in [0, T_{z_{vi0}})$, substituting the definition of ζ_{vi0}:

$$\dot{L}_{z_{vi0}} = -z_{vi0}\zeta_{vi0} = -\frac{k_{vi1}|z_{vi0}|(1+z_{vi0}^2)\arctan(|z_{vi0}|)}{T_{z_{vi0}}-t+k_{vi3}} \tag{82}$$

Defining the auxiliary variable $m_{vi3} = \sqrt{2L_{z_{vi0}}}$, the integration process mirrors Phase 1, proving that z_{vi0} and its associated energy function converge prior to $t = T_{z_{vi0}} + k_{vi3}$. Similarly, through the squeeze theorem, the state z_{vi0} reaches equilibrium exactly within the prescribed time.

Case 2: For $t \in [T_{z_{vi0}}, \infty)$, the derivative is bounded by:

$$\dot{L}_{z_{vi0}} \leq -2\left[\exp\left(\frac{\sqrt{k_{vi2}}}{k_{vi3}} - \frac{k_{vi2}}{t-T_{z_{vi0}}+\sqrt{k_{vi2}}k_{vi3}}\right) + \frac{k_{vi1}}{k_{vi3}} - 1\right] L_{z_{vi0}} \tag{83}$$

By applying Gronwall's lemma, the error state z_{vi0} is strictly constrained within a minuscule boundary, confirming the successful convergence of the observation error.

The ultimate objective is to prove the convergence of the lumped disturbance estimation error, defined as $\tilde{D}_{Vi} = D_{Vi} - \hat{D}_{Vi}$. From the auxiliary variable dynamics, the actual

total disturbance can be rewritten as: $D_{Vi} = l_{vi2}\vartheta_{vi} + l_{vi1}^{-1}\dot{\vartheta}_{vi}$. Simultaneously, the observer's output is: $\hat{D}_{Vi} = l_{vi2}\hat{\vartheta}_{vi} + l_{vi1}^{-1}\dot{\hat{\vartheta}}_{vi}$.

Subtracting the estimated value from the actual value yields the error dynamics as a linear combination of the state discrepancy $z_{vi0} = \vartheta_{vi} - \hat{\vartheta}_{vi}$:

$$\tilde{D}_{Vi} = l_{vi2}(\vartheta_{vi} - \hat{\vartheta}_{vi}) + l_{vi1}^{-1}(\dot{\vartheta}_{vi} - \dot{\hat{\vartheta}}_{vi}) = l_{vi2}z_{vi0} + l_{vi1}^{-1}\dot{z}_{vi0} \tag{84}$$

Based on the thorough derivations in the preceding steps, both the observation error z_{vi0} and its time derivative $\dot{z}_{vi0}$ converge to an infinitesimally small neighborhood of the origin within the total prescribed time horizon $T_{z_{vi0}} + T_{z_{vi1}}$. Consequently, it directly follows that $\tilde{D}_{Vi} \to 0$. This confirms the fast and precise estimation capability of the proposed sliding mode disturbance observer for the translational subsystem. This concludes the proof. □

3.2.2. Prescribed-Time Sliding Mode Controller

In the context of first-order systems, the construction of a conventional cascaded sliding manifold is obviated. Instead, we leverage the continuous and smooth properties of the RCDF to directly regulate the error dynamics $\dot{e}_{vi}$. By integrating this with feedforward compensation derived from the observer, the thrust control law is formulated as follows.

Theorem 5. *Regarding the velocity error dynamics, consider the control law designed as:*

$$F_{Txi0} = g_{vi}^{-1}\left(\dot{V}_d - f_{vi} - \hat{D}_{Vi} - \zeta_{vi}\right) \tag{85}$$

where ζ_{vi} denotes a continuous, piecewise prescribed-time convergence function, where

$$\zeta_{vi} = \begin{cases} \frac{\eta_{vi}(1+e_{vi}^2)\arctan(e_{vi})}{T_{vi}-t+\delta_{vi}} & 0 \le t < T_{vi} \\ \left[\exp\left(\frac{\sqrt{\sigma_{vi}}}{\delta_{vi}} - \frac{\sigma_{vi}}{t-T_{vi}+\sqrt{\sigma_{vi}}\delta_{vi}}\right) + \frac{\eta_{vi}}{\delta_{vi}} - 1\right]e_{vi} & t \ge T_{vi} \end{cases} \tag{86}$$

Under this control scheme, the closed-loop system exhibits global practical prescribed-time stability. The velocity tracking error e_{vi} is guaranteed to settle within a compact residual set centered at the origin by the pre-assigned time T_{vi}. Furthermore, this formulation inherently eliminates the chattering effect in the control input.

Proof of Theorem 5. To verify the stability of the translational subsystem and ensure consistency with the attitude control analysis, we propose the following composite Lyapunov candidate function $L_{vi} = \frac{1}{2}e_{vi}^2 + \frac{1}{2}z_{vi1}^2 + \frac{1}{2}z_{vi0}^2$. Taking the time derivative of L_{vi} along the system trajectories yields:

$$\begin{aligned} \dot{L}_{vi} &= e_{vi}\dot{e}_{vi} - \zeta_{vi1}z_{vi1} - \zeta_{vi0}z_{vi0} \\ &= e_{vi}(f_{vi} + g_{vi}F_{Txi0} + D_{Vi} - \dot{V}_d) - \zeta_{vi1}z_{vi1} - \zeta_{vi0}z_{vi0} \end{aligned} \tag{87}$$

By substituting the prescribed-time thrust command F_{Txi0} and the observer relations into the above, we obtain:

$$\begin{aligned} \dot{L}_{vi} &= e_{vi}(-\zeta_{vi} - \hat{D}_{Vi} + D_{Vi}) - \zeta_{vi1}z_{vi1} - \zeta_{vi0}z_{vi0} \\ &\le -e_{vi}\zeta_{vi} + \Pi_{vi} \end{aligned} \tag{88}$$

where Π_{vi} represents the bounded lumped terms associated with the observation errors and disturbances.

Case 1: For the reaching phase $t \in [0, T_{vi})$, utilizing the piecewise RCDF ζ_{vi}, the following inequality holds:

$$\begin{aligned} \dot{L}_{vi} &\leq -\frac{\eta_{vi} e_{vi}(1+e_{vi}^2)\arctan(e_{vi})}{T_{vi}-t+\delta_{vi}} + \Pi_{vi} \\ &\leq -\frac{\eta_{vi}|e_{vi}|(1+|e_{vi}^2|)\arctan(|e_{vi}|)}{T_{vi}-t+\delta_{vi}} + \Pi_{vi} \end{aligned} \tag{89}$$

To facilitate the subsequent stability analysis, we utilize the property $(1+\omega^2)\arctan(\omega) \geq \omega$. Invoking this property, the Lyapunov derivative is bounded by:

$$\dot{L}_{vi} \leq -\frac{\eta_{vi}}{T_{vi}-t+\delta_{vi}} e_{vi}^2 + \Pi_{vi} \tag{90}$$

Let us redefine the Lyapunov components as $V_{vi} = V_{vi1} + V_{vi2} = L_{vi}$, where $V_{vi1} = \frac{1}{2}e_{vi}^2$ and $V_{vi2} = \frac{1}{2}z_{vi1}^2 + \frac{1}{2}z_{vi0}^2$. Then, we arrive at the following constraint:

$$\begin{aligned} \dot{V}_{vi} &\leq -\frac{2\eta_{vi}}{T_{vi}-t+\delta_{vi}} V_{vi1} + \Pi_{vi} \\ &\leq -\frac{2\eta_{vi}}{T_{vi}-t+\delta_{vi}} V_{vi} + \frac{2\eta_{vi}}{T_{vi}-t+\delta_{vi}} V_{vi2} + \Pi_{vi} \end{aligned} \tag{91}$$

It can thus be concluded that V_{vi} remains bounded. By invoking the results from [37] and applying Gronwall's inequality, the following relationship is established:

$$\begin{aligned} V_{vi}(t) \leq\ & e^{-2\int_0^t \frac{\eta_{vi}}{T_{vi}-s+\delta_{vi}} ds} V_{vi}(0) + e^{-2\int_0^t \frac{\eta_{vi}}{T_{vi}-s+\delta_{vi}} ds} \\ & \int_0^t \left(\frac{2\eta_{vi}}{T_{vi}-\omega+\delta_{vi}} V_{vi2} + \Pi_{vi} \right) e^{2\int_0^\omega \frac{\eta_{vi}}{T_{vi}-s+\delta_{vi}} ds} d\omega \end{aligned} \tag{92}$$

As the time variable t approaches the pre-assigned threshold T_{vi}, it can be verified that the transient term associated with $V_{vi}(0)$ vanishes. Furthermore, by employing L'Hospital's rule to evaluate the limit, we demonstrate that:

$$\begin{aligned} \lim_{t\to T_{vi}} V_{vi} &\leq \lim_{t\to T_{vi}} \frac{\int_0^t \left(\frac{2\eta_{vi}}{T_{vi}-\omega+\delta_{vi}} V_{vi2} + \Pi_{vi} \right) e^{2\int_0^\omega \frac{\eta_{vi}}{T_{vi}-s+\delta_{vi}} ds} d\omega}{e^{2\int_0^t \frac{\eta_{vi}}{T_{vi}-s+\delta_{vi}} ds}} \\ &\leq \lim_{t\to T_{vi}} \left(V_{vi2} + \frac{(T_{vi}-t+\delta_{vi})\Pi_{vi}}{2\eta_{vi}} \right) = a_{vi1} \end{aligned} \tag{93}$$

This confirms that the state tracking error enters the bound a_{vi1} within the prescribed time horizon T_{vi}.

Case 2: For the steady-state phase $t \in [T_{vi}, +\infty)$, the evolution of the Lyapunov candidate is expressed as:

$$\begin{aligned} \dot{V}_{vi}(t) = \dot{V}_{vi1}(t) + \dot{V}_{vi2} &\leq -e_{vi}\zeta_{vi} + \Pi_{vi} \\ &\leq -2\eta_{vi}\left[\exp\left(\frac{\sqrt{\sigma_v i}}{\delta_{vi}} - \frac{\sigma_v i}{t - T_{vi} + \sqrt{\sigma_v i}\delta_{vi}} \right) + \frac{1}{\delta_{vi}} - 1 \right] V_{vi} \\ &\quad + 2\eta_{vi}\left[\exp\left(\frac{\sqrt{\sigma_v i}}{\delta_{vi}} - \frac{\sigma_v i}{t - T_{vi} + \sqrt{\sigma_v i}\delta_{vi}} \right) + \frac{1}{\delta_{vi}} - 1 \right] V_{vi2} + \Pi_{vi} \end{aligned} \tag{94}$$

As the time variable tends toward infinity ($t \to \infty$), the transient term associated with $V_{vi}(T_{vi})$ decays to zero. Thus, the steady-state bound is obtained as:

$$\begin{aligned} \lim_{t\to\infty} V_{vi}(t) &\leq V_{vi2} + \frac{\Pi_{vi}}{2\eta_{vi}\left[\exp\left(\frac{\sqrt{\sigma_{vi}}}{\delta_{vi}}\right) + \frac{1}{\delta_{vi}} - 1\right]} \\ &\leq \frac{\delta_{vi}\Pi_{vi}}{2\eta_{vi}\left[\delta_{vi}\exp\left(\frac{\sqrt{\sigma_{vi}}}{\delta_{vi}}\right) + 1 - \delta_{vi}\right]} = a_{vi2} \end{aligned} \tag{95}$$

In conclusion, the Lyapunov function V_{vi} is confirmed to be bounded, ensuring that the system trajectories converge to a predefined residual set within the specified time T_{vi} and remain stable thereafter. This concludes the proof. □

Remark 2. *As illustrated in (23) and (24), (40), (44), (74) and (75) and (86), the RCDF provides a more computationally efficient framework by combining a time-varying scaling function with the tracking error. This approach avoids the need for complex transition mechanisms and addresses tracking control across the entire temporal horizon. Following the insights in [31], the error convergence rate can be precisely modulated by adjusting the parameters.*

Remark 3. *The RCDF maintains continuity at the terminal time $t = T$, satisfying $\lim_{t\to T} \psi_{1.i2} = (T - t + \delta)^{\eta-1} = 0$. The asymptotic behavior is given by $\psi_i \sim (T - t + \delta)^{\eta-1}$ and $\psi_i^{(n-1)} \sim (T - t + \delta)^{\eta-n}$. Provided that the design parameters satisfy $\eta_i > n + 1 - i$, the derivatives of each ψ_i vanish as t tends toward T. Based on these properties, we define the unary mapping $h(v) = v\vartheta(v) = v(1 + kv^2)\arctan(v)$, which is proven to be a convex function. For a more comprehensive discussion, the reader is referred to [31].*

Remark 4. *While the theoretical analysis guarantees system stability within any user-defined prescribed time, the practical implementation on a QUAV is fundamentally constrained by physical actuator limits. In a real-world scenario, the required control effort is inversely proportional to the prescribed settling time. Consequently, two specific scenarios can lead to severe actuator saturation and increased failure risk: (1) setting an extremely short convergence time when the initial attitude error is excessively large; and (2) encountering a sudden, massive external disturbance during the flight, causing the controller to demand infinite torque to eliminate the newly generated error within a tightly constrained time window. Therefore, in practical engineering applications, the selection of prescribed time must not be arbitrary. It requires a cautious trade-off, ensuring that the maximum demanded control torque does not exceed the physical saturation threshold of the airframe's actuators, thereby preserving structural integrity and flight safety.*

4. Simulation Experiment

This section evaluates the proposed control strategy through numerical simulations, aimed at verifying its feasibility and performance advantages in practical cases.

Parameter Setting

According to existing work [36], to verify the effectiveness of the proposed control strategy, the parameters of the prescribed-time sliding mode disturbance observers and controllers are strictly set in the simulation, where the subscript $i \in \{1, 2, 3, 4\}$ denotes the four UAVs. The observer parameters of the attitude subsystem are identical for all UAVs, specifically chosen as $k_{\varphi 1i} = [45, 45, 45]^{\mathrm{T}}$, $k_{\varphi 2i} = [7, 7, 7]^{\mathrm{T}}$, $k_{\varphi 3i} = [1, 1, 1]^{\mathrm{T}}$, $k_{\varphi 4i} = [0.1, 0.1, 0.1]^{\mathrm{T}}$, $k_{\varphi 5i} = [15, 15, 15]^{\mathrm{T}}$, $k_{\varphi 6i} = [0.1, 0.1, 0.1]^{\mathrm{T}}$, $\boldsymbol{\kappa}_{\varphi 1i} = \mathrm{diag}(50, 50, 50)$, and $\boldsymbol{\kappa}_{\varphi 2i} = \mathrm{diag}(1, 1, 1)$; the attitude controller parameters are set as $\eta_{\varphi 1i} = [5, 5, 5]^{\mathrm{T}}$, $\eta_{\varphi 2i} = [7, 7, 7]^{\mathrm{T}}$, $\sigma_{\varphi 1i} = \sigma_{\varphi 2i} = [2, 2, 2]^{\mathrm{T}}$, and $\delta_{\varphi 1i} = \delta_{\varphi 2i} = [0.2, 0.2, 0.2]^{\mathrm{T}}$. The ob-

server parameters of the translational subsystem are configured as $k_{vi1} = 4$, $k_{vi2} = 0.5$, $k_{vi3} = 0.1$, $k_{vi4} = 4$, $k_{vi5} = 0.5$, $k_{vi6} = 0.1$, $l_{v1} = 50$, and $l_{v2} = 1$; its corresponding controller parameters are selected as $\sigma_{vi} = 7$, $\delta_{vi} = 3$, and $\eta_{vi} = 4$. To test the system robustness, continuous, time-varying, and non-vanishing external disturbances are introduced in the simulation. The disturbances injected into the attitude channels of the four UAVs are respectively set as $d_{\varphi 1} = [0.1\cos(0.5t), 0.1\cos(0.5t) + 0.1\sin(t), 0.1\sin(0.5t)]^{\mathrm{T}}$, $d_{\varphi 2} = 0.7[1 + \sin(0.3t) + \cos(0.8t), -1 + \sin(0.6t) - \cos(0.4t), 1 + \sin(0.5t) + \cos(0.2t)]^{\mathrm{T}}$, $d_{\varphi 3} = 0.5[0.7\sin(0.7t) + 3\cos(0.3t), \sin(0.9t) + 0.5\cos(0.4t), 1 + \sin(1.2t) + 0.7\cos(1.2t)]^{\mathrm{T}}$, and $d_{\varphi 4} = 0.6[1 + 1.2\sin(0.9t) + 0.8\cos(t), -1 + \sin(1.8t) - 1.5\cos(0.3t), 1 + 0.5\sin(0.5t) + 1.3\cos(0.2t)]^{\mathrm{T}}$; meanwhile, the uniform external disturbance acting on the translational subsystems is defined as $d_{vi} = 0.5[1 + 0.5sin(1.3t); 1 + 0.9sin(0.6t); 1 + 0.9cos(0.8t)]$;$^{\mathrm{T}}$. And the prescribed time is $T_{d_{\varphi i0}} = 4$ s, $T_{d_{\varphi i1}} = 4$ s, $T_{z_{\varphi i1}} = 6$ s, $T_{z_{\varphi i2}} = 6$ s, $T_{z_{v0i}} = 4$ s, $T_{vi} = 4$ s. Meanwhile, UAV 2 operates under healthy conditions without any actuator anomalies throughout the entire mission. Furthermore, we introduce an actuator fault case for UAV 1 within the time window $t \in [15, 20]$, affecting the elevator, rudder, and ailerons. This is represented by the bias $\boldsymbol{\delta}_{1f} = [0, 0.8, 0]^{\mathrm{T}}$ and the efficiency factor matrix $\boldsymbol{\varrho}_{\delta 1} = \mathrm{diag}\{0.8, 0.8, 0.8\}$. Similarly, we introduce an actuator fault case for UAV 3 within the time window $t \in [15, 25]$, affecting the elevator, rudder, and ailerons. This is represented by the bias $\boldsymbol{\delta}_{3f} = [0, 0.8, 0]^{\mathrm{T}}$ and the efficiency factor matrix $\boldsymbol{\varrho}_{\delta 3} = \mathrm{diag}\{0.85, 0.85, 0.85\}$. Finally, we introduce an actuator fault case for UAV 4 within the time window $t \in [10, 15]$, affecting the elevator, rudder, and ailerons. This is represented by the bias $\boldsymbol{\delta}_{4f} = [0, 0.8, 0]^{\mathrm{T}}$ and the efficiency factor matrix $\boldsymbol{\varrho}_{\delta 4} = \mathrm{diag}\{0.85, 0.85, 0.85\}$. The starting states for the formation are detailed in Table 2. The initial value of UAVs are shown in Table 3.

Table 2. Airframe parameter values of UAV.

Coefficient	Value	Unit	Coefficient	Value	Unit
g	9.8	$\mathrm{m \cdot s^{-2}}$	$\bar{\rho}$	1.29	$\mathrm{kg \cdot m^2}$
m_i	20.64	kg	S_i	1.37	$\mathrm{m^2}$
b_i	1.96	m	$\bar{c}_i$	0.76	m
c_{L0i}	0.1	/	$c_{L\alpha i}$	0.25	$\mathrm{rad^{-1}}$
c_{l0i}	−0.001	/	$c_{l\beta i}$	−0.038	$\mathrm{rad^{-1}}$
c_{D0i}	0.5	/	$c_{Y\beta i}$	−0.1	$\mathrm{rad^{-1}}$
c_{m0i}	0.022	/	$c_{m\alpha i}$	−0.473	$\mathrm{rad^{-1}}$
c_{n0i}	0.022	/	$c_{n\alpha i}$	0.036	$\mathrm{rad^{-1}}$
c_{lpi}	−0.213	$\mathrm{rad^{-1} \cdot s}$	c_{lri}	0.114	$\mathrm{rad^{-1} \cdot s}$
$c_{l\delta ai}$	−0.056	$\mathrm{rad^{-1}}$	$c_{l\delta ri}$	0.014	$\mathrm{rad^{-1}}$
$c_{n\delta ai}$	−0.036	$\mathrm{rad^{-1}}$	$c_{n\delta ri}$	−0.055	$\mathrm{rad^{-1}}$
c_{mqi}	−3.449	$\mathrm{rad^{-1} \cdot s}$	$c_{m\delta i}$	−0.364	$\mathrm{rad^{-1}}$
c_{npi}	−0.151	$\mathrm{rad^{-1} \cdot s}$	c_{nri}	−0.195	$\mathrm{rad^{-1} \cdot s}$
J_{xxi}	1.607	$\mathrm{kg \cdot m^2}$	J_{yyi}	7.51	$\mathrm{kg \cdot m^2}$
J_{zzi}	7.18	$\mathrm{kg \cdot m^2}$	J_{xzi}	0.59	$\mathrm{kg \cdot m^2}$

Table 3. Initial state values of UAV.

	$x_i(0)$	$y_i(0)$	$z_i(0)$	$\phi_i(0)$	$\theta_i(0)$	$\psi_i(0)$	$V_i(0)$
UAV 0	40 m	0 m	150 m	0°	1°	0°	20 m/s
UAV 1	10 m	−20 m	150 m	0.2°	1°	0°	25 m/s
UAV 2	10 m	20 m	150 m	1°	1°	0°	20 m/s
UAV 3	−10 m	−35 m	150 m	0°	1°	−0.5°	19.5 m/s
UAV 4	−10 m	35 m	150 m	0.2°	1.5°	−0.2°	15 m/s

The mission objective requires the multi-UAV system to execute a low-altitude traversal task while precisely following the prescribed velocity V_r and orientation $\boldsymbol{\varphi}_r$ profiles:

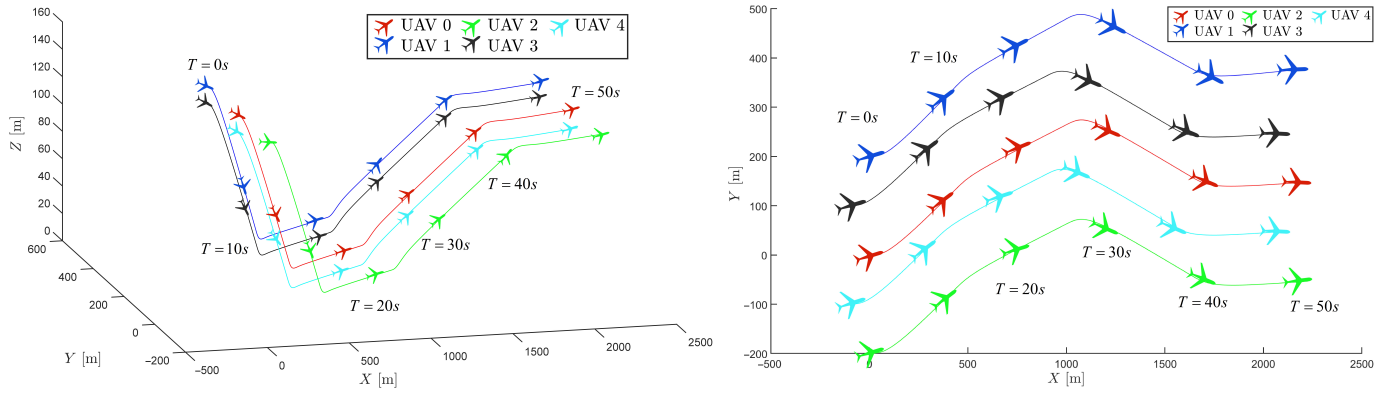
$$V_r = \begin{cases} 20 + \frac{30}{2s+1}, & 0\ \text{s} \le t < 10\ \text{s} \\ 20 + \frac{20}{0.4s+1}, & 10\ \text{s} \le t < 20\ \text{s} \\ 20 + \frac{30}{s+1}, & t \ge 20\ \text{s} \end{cases}, \quad \boldsymbol{\varphi}_r(t) = \begin{cases} [0,0,0]^{\mathrm{T}}, & 0\ \text{s} \le t < 5\ \text{s} \\ [0, \frac{-50}{1.5s+1}, 0]^{\mathrm{T}}, & 5\ \text{s} \le t < 20\ \text{s} \\ [0,0,0]^{\mathrm{T}}, & t \ge 20\ \text{s} \end{cases} \tag{96}$$

Figure 3 illustrates the flight trajectories of the fixed-wing UAV swarm in both a three-dimensional isometric view (Figure 3a) and a horizontal X-Y projection (Figure 3b). Under the proposed control scheme, the four follower UAVs successfully assemble and maintain the desired formation with the leader (UAV 0) throughout the complex traversal mission, which includes continuous maneuvering, climbing, and diving phases. Figure 4 further details the actual state trajectories of the UAVs across the speed (V_i), roll (ϕ_i), pitch (θ_i), and yaw (ψ_i) channels. The system states dynamically and smoothly follow the time-varying reference commands within the prescribed time. Notably, when the reference velocity V_r shifts at $t = 10$ s and $t = 20$ s, all UAVs adjust their speeds rapidly and uniformly, demonstrating the excellent transient performance of the velocity controller. Furthermore, despite the sequential injection of actuator faults across different UAVs, the state trajectories exhibit no noticeable oscillations or divergence. This directly infers the strong structural robustness of the proposed dual-channel control architecture against unexpected hardware anomalies. The dynamic evolution of the tracking errors ($e_{vi}, e_{\phi i1}, e_{\theta i1}, e_{\psi i1}$) is presented in Figure 5. Governed by the proposed controller, these errors converge to a small neighborhood near zero within the prescribed time, despite the continuous external disturbances. It is visually evident from the subgraphs that the convergence moments exactly align with the pre-set theoretical time boundaries, verifying that the settling time is strictly independent of initial conditions. Moreover, the error curves remain completely smooth after reaching the sliding phase, which physically confirms that the proposed continuous reference convergence differential function (RCDF) successfully eliminates the chattering phenomenon inherent in traditional sliding mode control. The efficacy of the prescribed-time sliding mode disturbance observer is evaluated in Figures 6–8. Figures 6 and 8a demonstrate that the estimated values closely track the actual time-varying lumped disturbances in both the attitude and translational subsystems. Correspondingly, Figures 7 and 8b confirm that the estimation errors ($\tilde{D}_{\varphi i}, \tilde{D}_{Vi}$) strictly converge within the prescribed estimation time. This rapid and accurate convergence ensures that the observer fully captures the complex aerodynamic variations well before the main controller's settling time. Consequently, this precise and timely feedforward compensation serves as the fundamental reason why the UAV swarm can maintain high-precision tracking without steady-state offsets under severe and non-vanishing disturbance.

In summary, the simulation results confirm that the integration of the proposed strategy provides robust, high-precision, and chattering-free tracking control for fixed-wing UAV swarms, effectively accommodating external disturbance and actuator fault within strict time constraints.

Remark 5. *Despite the robust tracking performance demonstrated under prescribed-time constraints, several limitations within the current study must be acknowledged. Firstly, the validation of the proposed control architecture currently relies on theoretical proofs and numerical simulations. While these simulations rigorously verify the mathematical stability bounds, they cannot fully capture the unmodeled physical aerodynamic complexities and sensor noise inherent in real-world environments. Thus, further empirical validation through extensive hardware-in-the-loop (HIL) testing using physical flight controllers, such as Pixhawk platforms, is required. Secondly, the proposed framework assumes an ideal, continuous transmission of reference states from the leader*

to the followers. In practical operational environments, communication delays and data packet losses between the leader and followers are inevitable, which could affect formation accuracy and the deterministic bounds of the prescribed time. Additionally, the current theoretical derivation does not explicitly account for absolute physical actuator saturation limits. Finally, the current scope is strictly confined to low-level continuous trajectory tracking and disturbance rejection. It does not yet integrate high-level intelligent autonomous decision-making or dynamic task allocation mechanisms, which are critical for the strategy generalization of large-scale UAV swarms. Addressing these constraints will be the primary focus of our subsequent research.



(**a**) (**b**)

Figure 3. Flight trajectories of the UAVs from different perspectives: (**a**) three-dimensional isometric view; (**b**) horizontal plane projection.

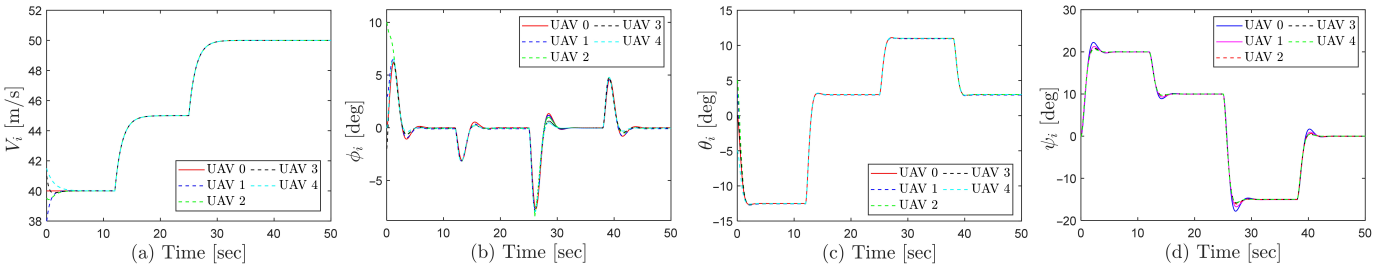


Figure 4. Actual states trajectories of UAVs: (**a**) speed channel; (**b**) ϕ channel; (**c**) θ channel; (**d**) ψ channel.

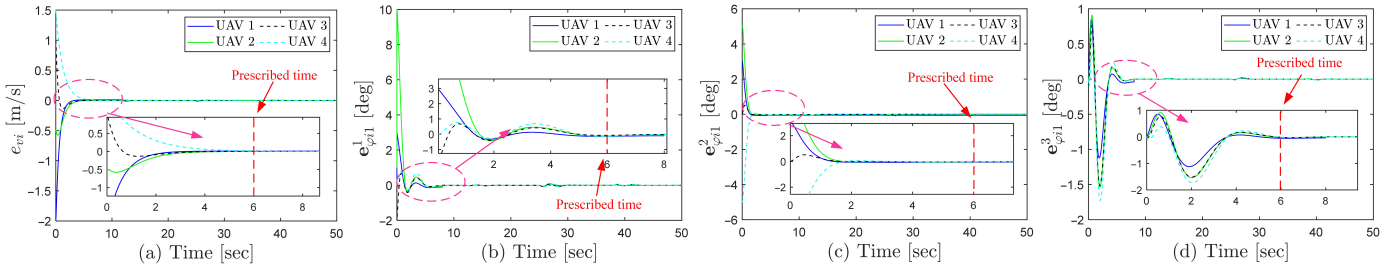


Figure 5. Tracking error of UAVs: (**a**) speed channel; (**b**) ϕ channel; (**c**) θ channel; (**d**) ψ channel.

https://doi.org/10.3390/machines14050543

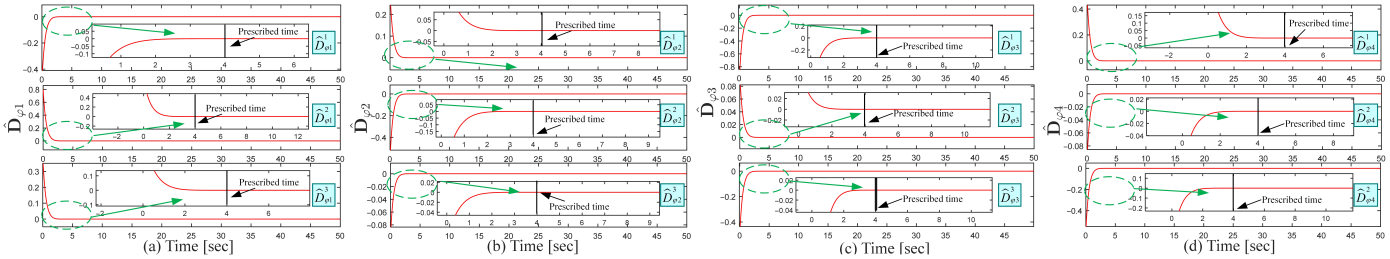


Figure 6. Estimated error of lumped disturbance in attitude subsystem: (**a**) UAV 1; (**b**) UAV 2; (**c**) UAV 3; (**d**) UAV 4.

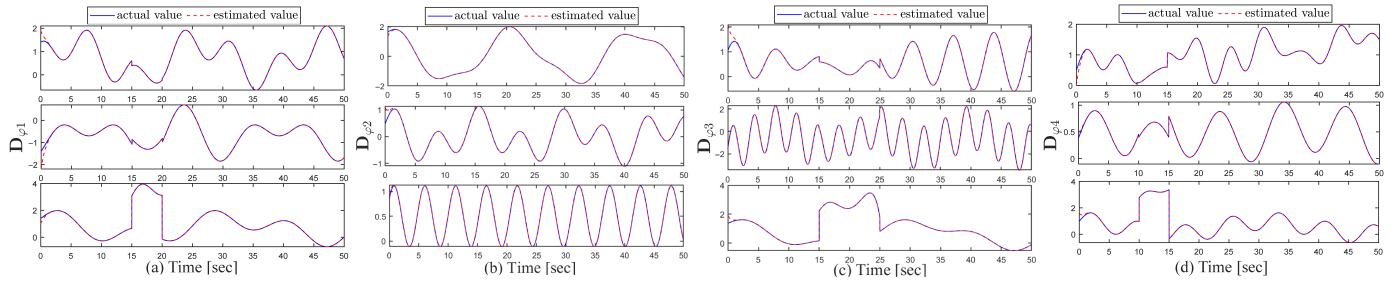


Figure 7. Estimated and actual value of lumped disturbance in attitude subsystem: (**a**) UAV 1; (**b**) UAV 2; (**c**) UAV 3; (**d**) UAV 4.

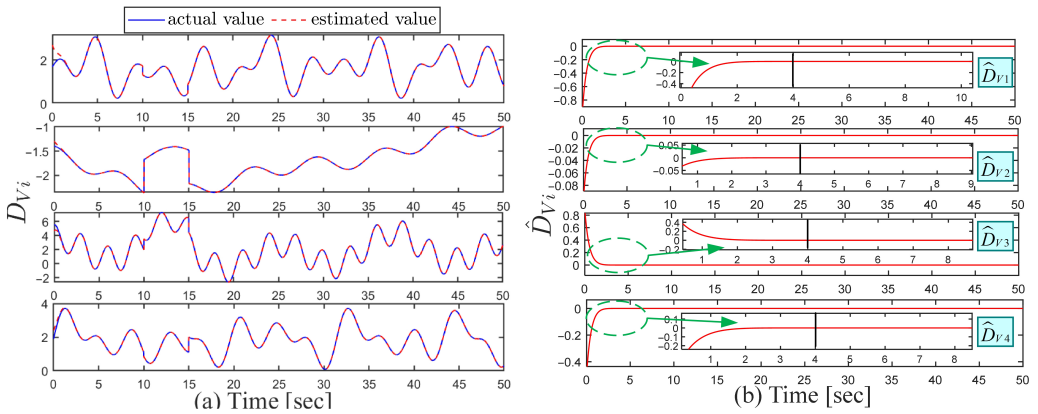


Figure 8. Lumped disturbance in translational subsystem: (**a**) estimated and actual value of UAVs; (**b**) Estimated error of UAVs.

5. Discussion and Conclusions

In this paper, a novel prescribed-time sliding mode control strategy integrated with a prescribed-time sliding mode disturbance observer (PTSMDO) has been successfully developed for the 6-DOF formation tracking of fixed-wing UAV swarms under non-vanishing external disturbances and actuator faults. Qualitatively, the introduction of a continuous and smooth piecewise reference convergence differential function (RCDF) effectively eliminates the need for complex state transitions and time-scaling functions. This design addresses the inherent singularity problems and ensures smooth, chattering-free control surface behavior across the entire temporal horizon. Consequently, the convergence rate is seamlessly modulated, and the tracking time is rendered completely independent of the system's initial conditions and environmental variations. Quantitatively, numerical simulations validate the strict exactness of the proposed architecture. The PTSMDO achieves highly accurate estimation of complex time-varying aerodynamic disturbances and actuator faults strictly within the user-defined timeframe of 4 s. Subsequently, the closed-loop controller drives all translational and attitude tracking errors into an infinitesimally small

neighborhood of zero within their respective prescribed times. Furthermore, the system demonstrates robust fault tolerance, maintaining tight formation bounds even when subjected to severe actuator anomalies. Ultimately, the proposed strategy provides a robust, computationally efficient, and high-precision solution for time-critical aerial swarm operations. Future work will focus on validating these theoretical results through extensive hardware-in-the-loop experiments under complex communication topologies.

Author Contributions: Conceptualization, G.L.; methodology, G.L. and M.L.; software (MATLAB R2022b), G.L.; validation, M.L.; resources, M.L.; writing original draft preparation, G.L. and M.L. All authors have read and agreed to the published version of the manuscript.

Funding: This research received no external funding.

Data Availability Statement: The original contributions presented in this study are included in the article. Further inquiries can be directed to the corresponding author.

Acknowledgments: The authors gratefully acknowledge the anonymous reviewers for their time, expertise, and invaluable feedback. Their insightful critiques and constructive suggestions were indispensable to achieving significant enhancements in the quality and rigor of this manuscript, and they are deeply appreciated.

Conflicts of Interest: The authors declare no conflicts of interest.

References

1. Oland, E.; Schlanbusch, R.; Kristiansen, R. Underactuated waypoint tracking of a fixed-wing UAV. *IFAC Proc. Vol.* **2013**, *46*, 126–133. [CrossRef]
2. Poksawat, P.; Wang, L.; Mohamed, A. Gain Scheduled Attitude Control of Fixed-Wing UAV with Automatic Controller Tuning. *IEEE Trans. Control Syst. Technol.* **2018**, *26*, 1192–1203. [CrossRef]
3. Song, Y.; Liu, Z.; Han, J.; Zhao, W.; Li, N. Coordinated Turn of Fixed-Wing Aircraft Under Wind Interface on Integral Backstepping. *IEEE Trans. Instrum. Meas.* **2021**, *70*, 2516718. [CrossRef]
4. Hu, S.; Ni, W.; Wang, X.; Jamalipour, A. Disguised Tailing and Video Surveillance with Solar-Powered Fixed-Wing Unmanned Aerial Vehicle. *IEEE Trans. Veh. Technol.* **2022**, *71*, 5507–5518. [CrossRef]
5. Jin, Z.; Bai, L.; Wang, Z.; Zhang, P. Self-Triggered Distributed Formation Control of Fixed-Wing Unmanned Aerial Vehicles Subject to Velocity and Overload Constraints. *IEEE Trans. Autom. Sci. Eng.* **2024**, *21*, 4082–4093. [CrossRef]
6. Tian, L.; Wang, X.; Chen, H. Heterogeneous Formation Tracking for Fixed-Wing UAVs and Nonholonomic UGVs with Different Asymmetric Constraints. *IEEE Trans. Veh. Technol.* **2025**, *74*, 13350–13360. [CrossRef]
7. Karpenko, M.; Nugaras, J. Vibration damping characteristics of the cork-based composite material in line with frequency analysis. *J. Theor. Appl. Mech.-Pol.* **2022**, *60*, 593–602. [CrossRef]
8. Karpenko, M.; Stosiak, M.; Deptuła, A.; Urbanowicz, K.; Nugaras, J.; Królczyk, G.; Żak, K. Performance evaluation of extruded polystyrene foam for aerospace engineering applications using frequency analyses. *Int. J. Adv. Manuf. Technol.* **2023**, *126*, 5515–5526. [CrossRef]
9. Zhang, B.; Hou, Y.; Yin, H.; Lv, M.; Yang, A.; Wu, L. Cooperative Dynamic Target Tracking: Distributed Time-Varying Optimization for Multi-UAV System. *IEEE Trans. Aerosp. Electron. Syst.* **2025**, *61*, 12245–12257. [CrossRef]
10. Shi, Y.; Li, J.; Lv, M.; Wang, N. A Dual-Layer Event-Triggered Framework for Distributed UAV Swarm Control. *IEEE Trans. Aerosp. Electron. Syst.* **2026**, *62*, 3798–3811. [CrossRef]
11. Bai, H.; Dong, J. Dynamic Deep ESN-Enhanced PID Optimization and Incremental Saturation Control Allocation for UAVs Under Actuator Faults. *IEEE Trans. Intell. Veh.* **2025**, *10*, 3082–3092. [CrossRef]
12. Abro, G.E.M.; Abdallah, A.M. Swarm Coordination and Trajectory Tracking in Quadrotor UAVs Using Fractional-Order PID Control Strategy. *IEEE Trans. Autom. Sci. Eng.* **2026**, *23*, 2995–3008. [CrossRef]
13. Wu, D.; Wang, M.; Zhang, Y.; Zhang, W.; Lippiello, V.; Siciliano, B. Distributed Neural Network Controller Based on Feature Enhancement with Flexible Time Prescribed Performance for Multi-UAV Swarms. *IEEE Trans. Aerosp. Electron. Syst.* **2025**, *61*, 8198–8209. [CrossRef]
14. Kang, H.H.; Ahn, C.K. Distributed Finite Memory Online Learning Strategy for Multi-UAV Systems with Neural Networks. *IEEE Trans. Ind. Electron.* **2025**, *72*, 919–927. [CrossRef]
15. Zhang, B.; Lv, M.; Cui, S.; Bu, X.; Park, J.H. Learning-Based Optimal Cooperative Formation Tracking Control for Multiple UAVs: A Feedforward-Feedback Design Framework. *IEEE Trans. Autom. Sci. Eng.* **2025**, *22*, 11–23. [CrossRef]

16. Shi, Y.; Li, J.; Lv, M.; Wang, N. Event-Based Fuzzy Asynchronous Consensus for UAV Swarm Under Jointly Connected Digraphs. *IEEE Trans. Fuzzy Syst.* **2025**, *33*, 3195–3209. [CrossRef]
17. Yu, L.; He, G.; Wang, X.; Zhao, S. Robust Fixed-Time Sliding Mode Attitude Control of Tilt Trirotor UAV in Helicopter Mode. *IEEE Trans. Ind. Electron.* **2022**, *69*, 10322–10332. [CrossRef]
18. Lian, S.; Meng, W.; Shao, K.; Zheng, J.; Zhu, S.; Li, H. Full Attitude Control of a Quadrotor Using Fast Nonsingular Terminal Sliding Mode with Angular Velocity Planning. *IEEE Trans. Ind. Electron.* **2023**, *70*, 3975–3984. [CrossRef]
19. Xiong, J.J.; Guo, N.H.; Mao, J.; Wang, H.D. Self-Tuning Sliding Mode Control for an Uncertain Coaxial Octorotor UAV. *IEEE Trans. Syst. Man Cybern. Syst.* **2023**, *53*, 1160–1171. [CrossRef]
20. Liu, B.; Wang, Y.; Sepestanaki, M.A.; Pouzesh, M.; Mobayen, S.; Rouhani, S.H. Event-Trigger-Based Adaptive Barrier Function Higher-Order Global Sliding Mode Control Technique for Quadrotor UAVs. *IEEE Trans. Aerosp. Electron. Syst.* **2024**, *60*, 5674–5684. [CrossRef]
21. Yin, T.; Gu, Z.; Xie, X. Observer-Based Event-Triggered Sliding Mode Control for Secure Formation Tracking of Multi-UAV Systems. *IEEE Trans. Netw. Sci. Eng.* **2023**, *10*, 887–898. [CrossRef]
22. Liu, B.; Wang, Y.; Mofid, O.; Mobayen, S.; Khooban, M.H. Barrier Function-Based Backstepping Fractional-Order Sliding Mode Control for Quad-Rotor Unmanned Aerial Vehicle Under External Disturbances. *IEEE Trans. Aerosp. Electron. Syst.* **2024**, *60*, 716–728. [CrossRef]
23. Lan, T.; Song, J.; Hou, Z.; Chen, K.; He, S.; Wang, H. Event-Triggered Fixed-Time Sliding Mode Control for Lip-Reading-Driven UAV: Disturbance Rejection Using Wind Field Optimization. *IEEE Trans. Autom. Sci. Eng.* **2025**, *22*, 9090–9103. [CrossRef]
24. Lian, S.; Zhu, Y.; Meng, W.; Shao, K.; Li, H. Adaptive Fault-Tolerant Control for Quadrotor Based on the Second-Order Fast Nonsingular Terminal Sliding Mode Control. *IEEE Trans. Ind. Electron.* **2025**, *72*, 8322–8332. [CrossRef]
25. Song, Y.; Wang, Y.; Holloway, J.; Krstic, M. Time-varying feedback for regulation of normal-form nonlinear systems in prescribed finite time. *Automatica* **2017**, *83*, 243–251. [CrossRef]
26. Shi, S.; Dai, L.; Min, H.; Hu, Y. Non-singular terminal sliding mode controller design for nonlinear systems with prescribed convergence time guarantees. *Int. J. Robust Nonlinear Control* **2023**, *34*, 2597–2613. [CrossRef]
27. Gao, Z.; Zhang, Y.; Guo, G. Prescribed-time control of vehicular platoons based on a disturbance observer. *IEEE Trans. Circuits Syst. II Express Briefs* **2022**, *69*, 3789–3793. [CrossRef]
28. Cui, B.; Wang, Y.; Liu, K.; Xia, Y. Sliding mode based prescribed-time consensus tracking control of second-order multi-agent systems. *Automatica* **2023**, *158*, 1111296. [CrossRef]
29. Shi, S.; Dai, L.; Min, H.; Yang, J.; Li, S. Prescribed-time nonsingular terminal sliding mode control and its application in PMSM servo systems. *IEEE Trans. Ind. Electron.* **2024**, *73*, 3072–3081. [CrossRef]
30. Ding, C.; Ding, S.; Mei, K. Adaptive prescribed-time SOSM controller design for nonlinear systems with prescribed performance. *IEEE Trans. Circuits Syst. II Express Briefs* **2024**, *71*, 1311–1315. [CrossRef]
31. Kuang, J.; Gao, Y.; Sun, Y.; Liu, A.; Liu, J. Stabilization with prescribed instant via Lyapunov method. *IEEE/CAA J. Autom. Sin.* **2024**, *11*, 557–559. [CrossRef]
32. Sun, J.; Yi, J.; Pu, Z.; Tan, X. Fixed-time sliding mode disturbance observer-based non-smooth backstepping control for hypersonic vehicles. *IEEE Trans. Syst. Man Cybern. Syst.* **2020**, *50*, 4377–4386. [CrossRef]
33. Zhao, L.; Li, Z.; Li, H.; Liu, B. Backstepping integral sliding mode control for pneumatic manipulators via adaptive extended state observers. *ISA Trans.* **2024**, *144*, 374–384. [CrossRef]
34. Song, T.; Fang, L.; Zhang, Y.; Shen, H. Recursive terminal sliding mode-based control of robot manipulators with a novel sliding mode disturbance observer. *Nonlinear Dyn.* **2024**, *112*, 1105–1121. [CrossRef]
35. Liu, L.; Dong, H.; Xu, X.; Tan, Z.; Geng, J.; Liu, B. Improved sliding mode disturbance observer-based model-free finite-time terminal sliding mode control for IPMSM speed ripple minimization. *Control Eng. Pract.* **2025**, *155*, 106178. [CrossRef]
36. Campa, G.; Gu, Y.; Seanor, B.; Napolitano, M.R.; Pollini, L.; Fravolini, M.L. Design and flight-testing of non-linear formation control laws. *Control Eng. Pract.* **2007**, *15*, 1077–1092. [CrossRef]
37. Luo, D.; Wang, Y.; Song, Y. Practical prescribed time tracking control with bounded time-varying gain under non-vanishing uncertainties. *IEEE/CAA J. Autom. Sin.* **2024**, *11*, 219–230. [CrossRef]
38. Briat, C. Convergence and equivalence results for the Jensen's Inequality Application to time-delay and sampled-data systems. *IEEE Trans. Autom. Control* **2011**, *56*, 1660–1665. [CrossRef]
39. Ning, P.; Hua, C.; Li, K.; Meng, R. Event-triggered control for nonlinear uncertain systems via a prescribed-time approach. *IEEE Trans. Autom. Control* **2023**, *68*, 6975–6981. [CrossRef]

Disclaimer/Publisher's Note: The statements, opinions and data contained in all publications are solely those of the individual author(s) and contributor(s) and not of MDPI and/or the editor(s). MDPI and/or the editor(s) disclaim responsibility for any injury to people or property resulting from any ideas, methods, instructions or products referred to in the content.